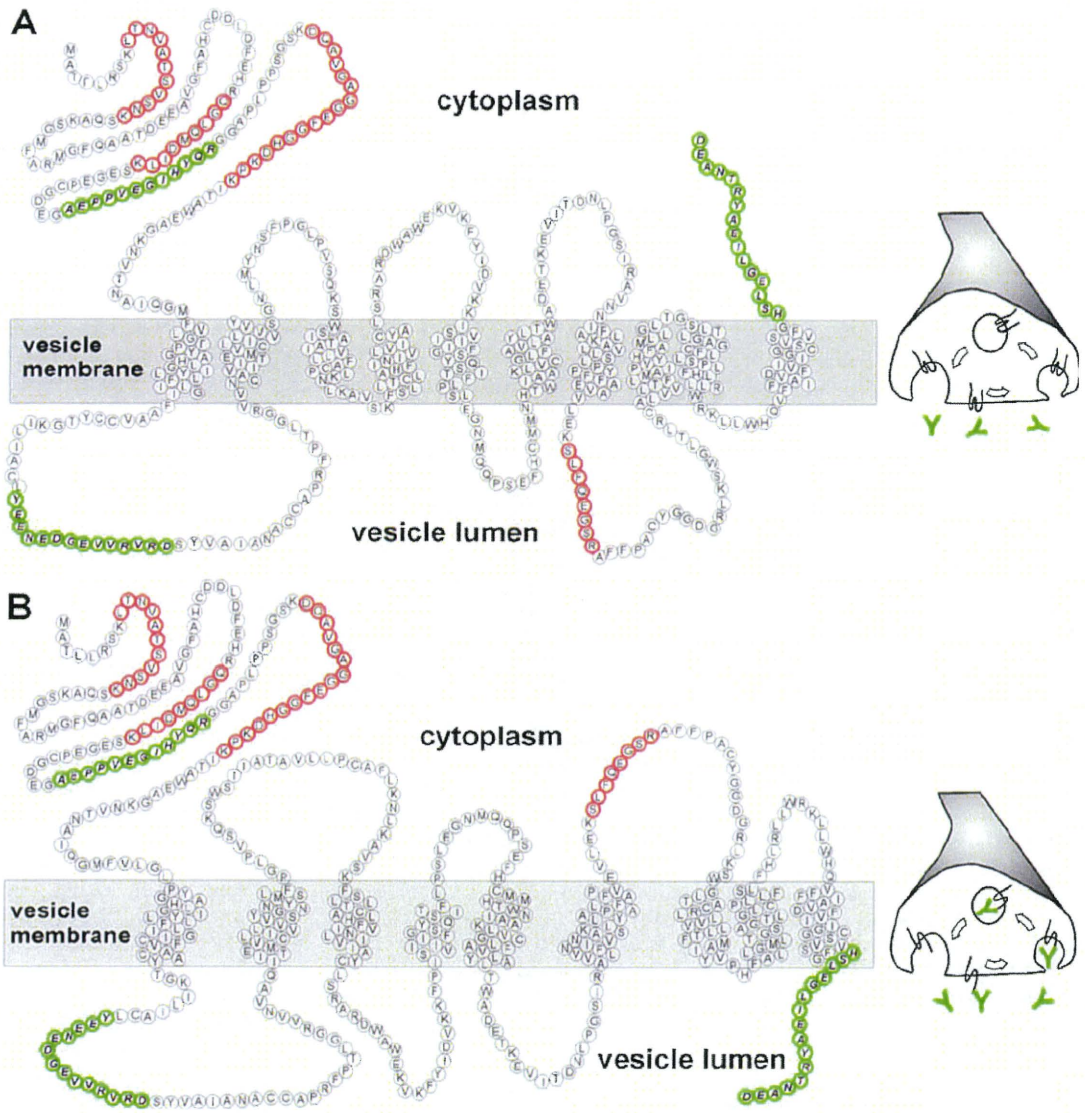

Figure 1. Refined transmembrane topology of VGAT. ***A***, Transmembrane structure of VGAT as proposed by McIntire et al. (1997) and as predicted by the TMHMM algorithm (***B***). Transmembrane domains are marked in gray. Epitopes in green were used to produce antibodies. Epitopes in red were detected by mass spectrometry. Insets denote the predicted exposure of luminal VGAT epitopes at the plasmalemmal surface and the likelihood of their targeting by antibodies during SV recycling.

e.g., the N terminus of Syt1 (Perin et al., 1991), are resistant to proteolytic cleavage as revealed by the molecular sizes of protected fragments by Western blotting (Stenius et al., 1995). In contrast, epitopes localized to the outer SV surface facing the cytosol, e.g., the N- and C-terminal endings of synaptogyrin and synaptophysin, are degradable. Here, we demonstrate that the C terminus of VGAT folds into the SV lumen. We also developed antibodies against short peptide sequences in (1) the N terminus, (2) the C terminus, or (3) the first luminal loop of VGAT (VGAT-N, VGAT-C, VGAT-lum1, respectively) (see Fig. 1) to elucidate the membrane topology of this protein, and to visualize forebrain GABAergic synapses both *in vitro* and *in vivo*. Similar to antibodies specific for the luminal domain of Syt1, which access the epitope during SV fusion and label endocytic vesicles (Kraszewski et al., 1995), fluorescent anti-VGAT-C targeting an intravesicular epitope allows the selective labeling of inhibitory presynaptic SV clusters during synaptic activity. Patch-clamp electrophysiology supports that anti-VGAT-C selectively recognizes VGAT. Collectively, our data elucidate a refined VGAT transmembrane topology and show that selective targeting of intraluminal VNT epitopes provides novel, effective means to label synapses of living neurons to establish their neurotransmitter phenotype *in vivo*.

Materials and Methods

Topology predictions. Transmembrane domain predictions were performed using default settings of the TMHMM (Center for Biological Sequence Analysis, Technical University of Denmark, Lyngby, Denmark; http://www.cbs.dtu.dk/services/TMHMM) and HMMTOP algorithms (Hungarian Academy of Sciences, http://www.enzim.hu/hmmtop/), and the Tmpred service (http://www.ch.embnet.org/software/TMPRED_form.html). Models were compared with the structure reported by McIntire et al. (1997). Theoretical molecular weights of proteins and proteolytic fragments were calculated with the ProtParam tool (www.expasy.org; Swiss Institute of Bioinformatics, Basel, Switzerland).

Antibodies and fluorochromation. Commercially available antibodies are listed in supplemental material, available at www.jneurosci.org. Peptides corresponding to AA 510–525 (anti-VGAT-C) and AA 171–184 (anti-VGAT-lum1) of rat VGAT (McIntire et al., 1997) were synthesized

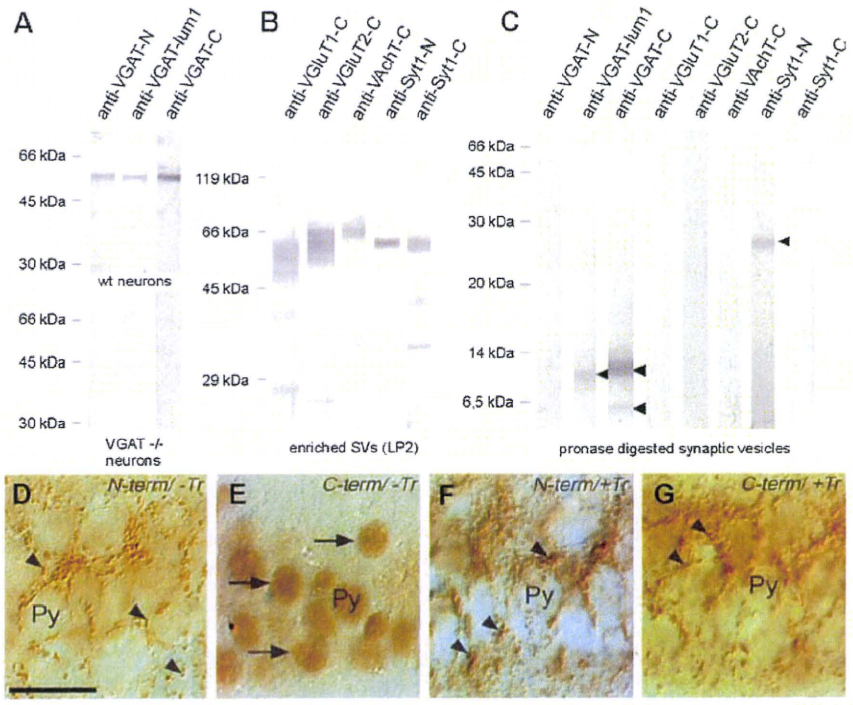

Figure 2. Epitope mapping of VGAT using domain-specific antibodies and limited SV proteolysis. ***A***, Comparison of antibodies raised against the N (VGAT-N) and C termini (VGAT-C), and the first luminal domain (VGAT-lum1) of VGAT by Western blotting of cell lysates from cultured wild-type (wt) and VGAT $^{-/-}$ hippocampal neurons. ***B***, Western analysis of enriched SVs (LP2) with antibodies recognizing the C termini of VGLUT1, VGLUT2, VAChT, the luminal N terminus (Syt1-N) and the cytoplasmic C terminus (Syt1-C) of Syt1. ***C***, Western analysis of proteolytic fragments (arrowhead) after pronase treatment of SVs. ***D–G***, Immunoperoxidase staining of VGAT-N and -C in hippocampal sections when luminal epitopes are concealed from or exposed to antibodies. Punctate terminal-like staining was detected around unstained pyramidal cells (Py) in the CA1 region by anti-VGAT-N both in the absence and presence of a detergent, respectively (arrowheads) (***D***, ***F***). Under identical staining conditions, anti-VGAT-C failed to reveal any terminal-like staining in the absence of a detergent even at high antibody concentrations causing aspecific nuclear staining (arrows) (***E***). Immunoperoxidase staining for VGAT-C with Triton X-100, which solubilizes membranes and facilitates antibody penetration into SV lumen, shows a punctate staining pattern resembling that obtained by anti-VGAT-N (***G***). Scale bar, 25 μm.

and coupled to keyhole limpet hemocyanin using standard procedures (Schneider et al., 1983). Antibodies were custom-generated (Biogenes) and affinity-purified using antigenic peptides immobilized on Sulfo-Link-Sepharose (Perbio) and are available from Synaptic Systems. Fluorochromation of affinity-purified anti-VGAT-C was performed following the manufacturers protocols (see supplemental material, available at www.jneurosci.org).

Biochemistry. Fractions enriched in synaptic vesicles (LP2) and pure SVs were prepared from adult Wistar rat brains according to Nagy et al. (1976). SDS-PAGE was used to detect full-length proteins (Laemmli, 1970). Pronase-digested SVs were separated by tricine SDS-PAGE to improve resolution in the low molecular range (Schägger and von Jagow, 1987). Each sample contained 200 μg of LP2 or 100 μg of pronase-treated SVs. Purified SVs (1 mg) were proteolytically digested with 200 μg of pronase (Sigma) in 2.5 ml of PBS (0.05 M, pH 7.4) for 3 h. Reactions were terminated by boiling the samples in SDS sample buffer containing 3% β-mercaptoethanol. Western blotting was performed according to Towbin et al. (1979). Mass spectrometry is described in supplemental material, available at www.jneurosci.org.

Immunoperoxidase staining. Immunoperoxidase staining of free-floating Vibratome sections was performed according to Chaudhry et al. (1998) (supplemental material, available at www.jneurosci.org).

Cell culturing and VGAT uptake. Primary hippocampal neurons were cultured according to Gauthier-Campbell et al. (2004). Internalization of fluorochromated antibodies was initiated by incubating neurons in Krebs-Ringer solution containing 55 mM KCl (Kraszewski et al., 1995) and polyclonal anti-VGAT-N, anti-VGAT-C or anti-VGAT-lum1 antibodies (5 μg/ml) at 37°C for 5 min. Cells were repeatedly washed in Krebs-Ringer buffer and subsequently in PBS. Images showing primary fluorochromated antibody binding were captured immediately. Unlabeled primary antibodies were detected after immersion fixation in 4% paraformaldehyde in PBS, blocking and permeabilization with PBS containing 3% BSA and 0.1% Triton X-100 for 20 min, and exposure to Cy3-tagged goat anti-rabbit IgG (1 h, 10–20 μg/ml, Jackson ImmunoResearch). Specific labeling was confirmed by co-staining with monoclonal anti-VGAT-N and Cy5-conjugated goat anti-mouse IgG. Details of CypHer5E-anti-VGAT-C uptake are in supplemental material, available at www.jneurosci.org.

Electrophysiology. Whole-cell patch-clamp recordings in hippocampal and striatal island cultures prepared from P0 mice were made according to Pyott and Rosenmund (2002) (supplemental material, available at www.jneurosci.org).

In vivo *labeling.* GABAergic terminals were labeled by stereotaxic injection of anti-VGAT-C into the hippocampi of anesthetized (33 μg/g; Hypnomidate, Janssen) young adult C57BL/6N mice. Surgery was performed as described (Siegemund et al., 2006) with 4 μg/2 μl anti-VGAT-C antibody injected at coordinates: AP = −2.2 mm, L = 1.9 mm, DV = 1.75 mm (relative to bregma). Mice were transcardially perfused 48 h later, and tissues processed according to Siegemund et al. (2006). *In vivo* labeling was analyzed in 30-μm-thick frozen sections as previously described for cholinergic neurons (Härtig et al., 1998). Labeling specificity was assessed by colocalization of Cy3- or Oyster550-anti-VGAT-C (2 μg/ml) and glutamate decarboxylase (GAD; 1:500), VGAT-N (1:50), parvalbumin (1:300) or synaptophysin (1:500; monoclonal IgGs). The absence of nonspecific *in vivo* labeling of glutamatergic fibers was shown by using guinea pig-anti-VGLUT1 (1:500; supplemental Table 1, available at www.jneurosci.org as supplemental material).

Results

Refined VGAT topology and verification by pronase mapping and mass spectrometry

McIntire et al. (1997) initially suggested a transmembrane VGAT structure with both termini facing the cytoplasm (Fig. 1*A*). Based on the TMHMM algorithm, we predicted an alternative transmembrane topology with the C terminus residing in the SV lumen being transiently exposed on the extracellular plasmalemmal surface during exocytotic fusion of SVs (Fig. 1*B*). We verified the transmembrane structure of VGAT by protease treatment of SVs followed by immunoblot analysis of the resulting fragments using epitope-mapped VGAT-N, VGAT-C and VGAT-lum1 antibodies (Fig. 1). Luminal, N- and cytoplasmic C-terminal tails of Syt1, and the C termini of VGLUT1, VGLUT2 and VAChT served as controls. Specificity of antibodies directed against three different epitopes of VGAT was confirmed by the findings that they recognized identical bands on cultured wild-type neurons but not on VGAT $^{-/-}$ material (Fig. 2*A*). Antibodies against VGLUT1, VGLUT2, VAChT and Syt1 revealed bands at the predicted molecular sizes (Perin et al., 1991, Stenius et al., 1995, Taka-

mori et al., 2000) in fractions enriched in synaptic vesicles (LP2) (Fig. 2*B*). Pronase treatment led to the loss of the VGAT-N epitope (Fig. 2*C*). In contrast, probing of blots with anti-VGAT-C (AA 510–525) and anti-VGAT-lum1 (AA171–184) yielded distinct bands showing that the epitopes were protected against proteolysis within the SV lumen (Fig. 2*C*). Because pronase treatment degrades all regions exposed on the vesicle surface, our refined topology model (Fig. 1*B*) predicts peptide fragments of 10.4 kDa and 3.9 kDa for the anti-VGAT-lum1 and anti-VGAT-C, respectively. Indeed, anti-VGAT-lum1 detected a proteolytic fragment of the expected size. However, the major protected C-terminal fragment migrated as a ~12 kDa protein while only a weaker signal of the expected size was detectable. No signals were obtained after pronase treatment with antibodies directed against the C termini of VGLUT1, VGLUT2 and VAChT, in agreement with their predicted cytoplasmic localization.

To confirm that intravesicular epitopes remained protected during pronase treatment we monitored the cleavage of Syt1 using antibodies specific for the N-terminal intraluminal and C-terminal cytoplasmic domains, respectively. While the cytoplasmic epitope was lost, a fragment of the expected size was detected by the N-terminal antibody (Fig. 2*C*). Furthermore, trypsin treatment coupled with mass spectrometry of digested fragments revealed four additional cytosolic peptide fragments (supplemental Fig. 1, available at www.jneurosci.org as supplemental material). Three of these fragments covered the cytosolic N terminus while one corresponds to the third cytoplasmic loop (Fig. 1*B*; supplemental Fig. 1, available at www.jneurosci.org as supplemental material) thus lending further support to our refined model of VGAT topology.

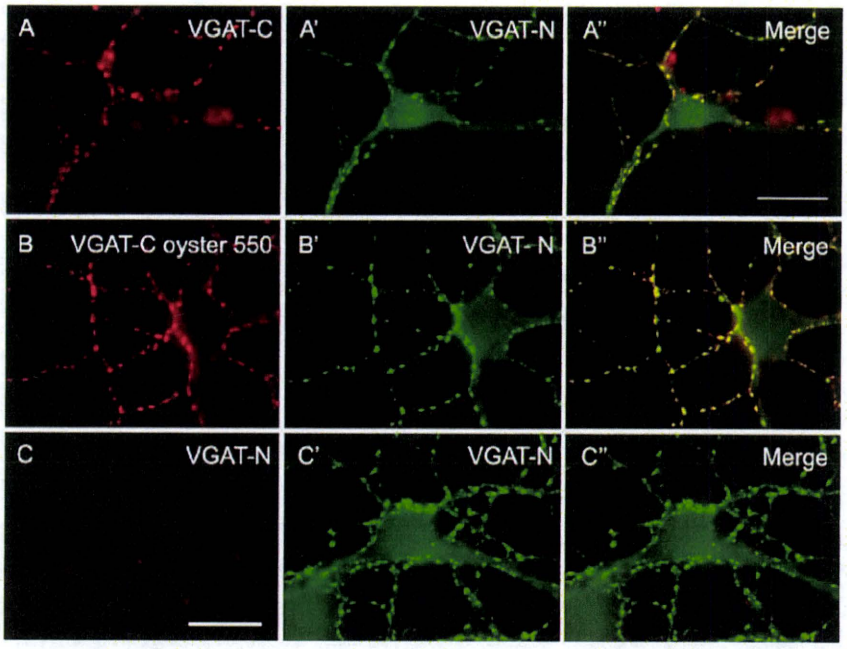

Figure 3. Labeling of live GABAergic neurons with anti-VGAT-C. ***A–A''***, Uptake of anti-VGAT-C at inhibitory terminals stimulated by 55 mM K^+. Incorporated antibodies were visualized after fixation and permeabilization by indirect immunofluorescence. Note prominent colocalization with anti-VGAT-N. ***B–B''***, Detection of inhibitory axon terminals through uptake of Oyster550-anti-VGAT-C of live rat hippocampal neurons *in vitro*. Anti-VGAT-N was applied indirectly on fixed cells. ***C–C''***, Control showing the lack of anti-VGAT-N uptake (cytoplasmic epitope) by cultured hippocampal neurons; subsequent counterstaining with monoclonal anti-VGAT-N. Yellow/orange color denotes colocalization. Scale bar, 20 μm.

Histochemical localization of VGAT C terminus

Immunoperoxidase (Fig. 2*D–G*) and immunofluorescence (supplemental Fig. 2, available at www.jneurosci.org as supplemental material) histochemistry of free-floating vibratome sections processed with or without detergent was performed to confirm the native folding of the two termini of VGAT across SV membranes. Since synapses at the tissue surface are cut open by the vibratome blade antibodies can directly access the surface of SVs (Chaudhry et al., 1998). In the absence of a detergent, anti-VGAT-N reveals punctate terminal-like staining concentrated e.g., in the hippocampal pyramidal cell layer (Fig. 2*D*) given its free access to the cytosolic VGAT N terminus (Boulland et al., 2008). In contrast, anti-VGAT-C failed to reveal any punctate staining even at high concentrations that otherwise lead to unspecific nuclear staining (Fig. 2*E*). Terminal-like labeling with anti-VGAT-C when its penetration is facilitated by Triton X-100 bolsters a luminal localization of this epitope (Fig. 2*F, G*). Immunofluorescence labeling and laser-scanning microscopy yielded identical results (supplemental Fig. 2, available at www.jneurosci.org as supplemental material). Overall, these data demonstrate that the C terminus of VGAT is localized in the lumen of SVs.

Dynamic labeling of GABAergic synapses *in vitro*

During recycling of SVs, luminal epitopes of SV proteins are temporarily exposed at the cell surface. Proteins recognizing these epitopes can bind to the surface of intact neurons and may become internalized by endocytosis. Indeed, antibodies directed against the N-terminal domain of Syt1 are widely used to selectively label recycling vesicles in nerve terminals (Kraszewski et al., 1995). Therefore, we tested whether anti-VGAT-C can be used to selectively label GABA release sites.

Immunohistochemistry on perfusion-fixed brain sections showed that both unlabeled and Oyster550-labeled anti-VGAT-C selectively recognize GABAergic axon terminals (supplemental Fig. 3, available at www.jneurosci.org as supplemental material). Next, we incubated live neurons for 5 min with anti-VGAT-C (5 μg/ml) with or without Oyster550 label at 37°C. Upon K^+-induced depolarization, bright immunofluorescence reminiscent of synaptic puncta were observed (Fig. 3*A,B*). Selective targeting of unlabeled anti-VGAT-C-derived (Fig. 3*A*) or Oyster550-anti-VGAT-C (Fig. 3*B*) to GABAergic synapses was verified by colocalization with anti-VGAT-N. Negligible or no labeling of inhibitory terminals was obtained by applying either cytoplasmic anti-VGAT-N (Fig. 3*C*) or anti-VGAT-lum1 (data not shown). Application of a CypHer5E-anti-VGAT-C conjugate that only produces fluorescence signal in endocytic vesicles at acidic pH also revealed terminal labeling (supplemental Fig. 4, available at www.jneurosci.org as supplemental material). These data reinforce the luminal localization of VGAT C terminus and its accessibility to antibodies in active synapses.

To verify that Oyster550-anti-VGAT-C is selectively taken up by GABAergic synapses, antibody- and mock-treated autaptic cultures

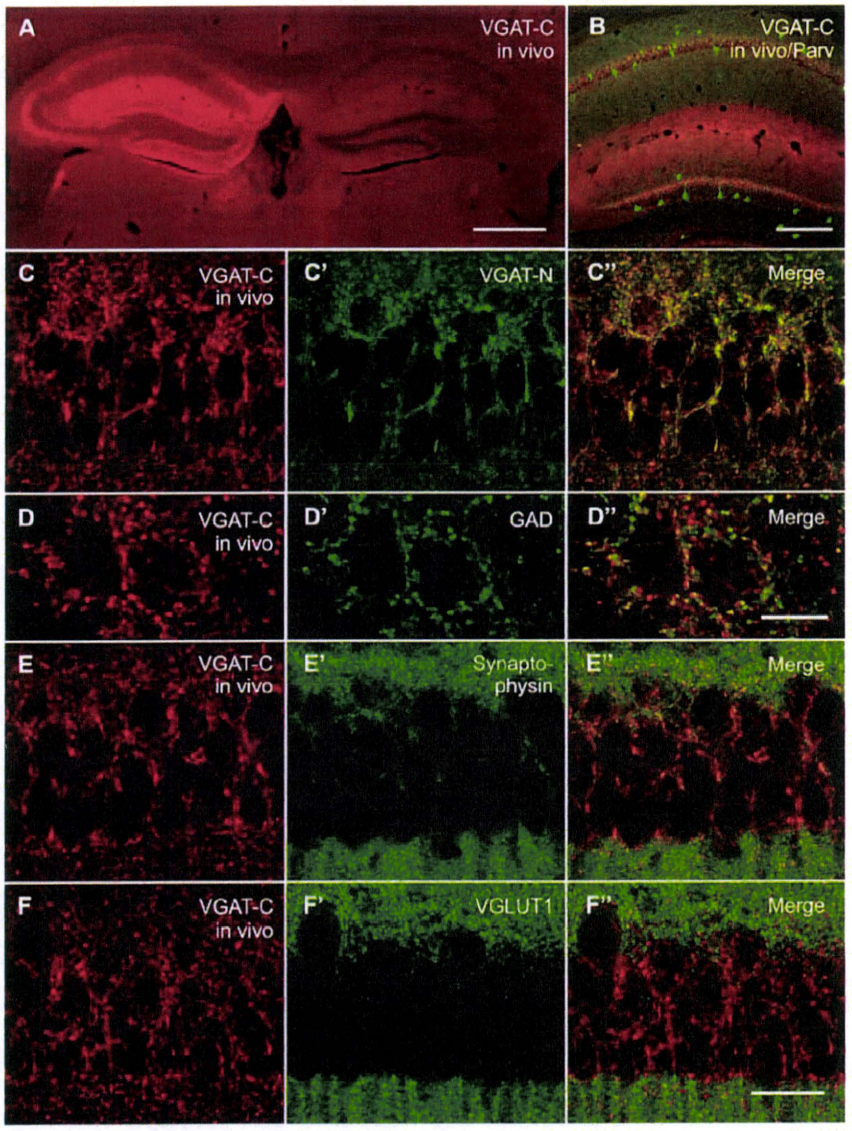

Figure 4. *In vivo* labeling of GABAergic synapses in mouse hippocampus. Direct *in vivo* VGAT-C labeling in the CA1 region and dentate gyrus (DG) 48 h after intrahippocampal antibody infusion combined with indirect Cy2-immunostaining of parvalbumin, VGAT-N, GAD, synaptophysin, and VGLUT1. ***A***, Distribution of Oyster550-anti-VGAT-C in the injected (left) hippocampal hemisphere. ***B***, Cy3-anti-VGAT-C in the injected hippocampal hemisphere counterstained with antibodies against parvalbumin. ***C–C″***, Oyster550-anti-VGAT-C counterstained with anti-VGAT-N in the CA1 region and combined with anti-GAD in DG (***D–D″***). Partial coexpression of Oyster550-anti-VGAT-C and synaptophysin in select GABAergic synapses (***E–E″***). Lack of coexistence of Oyster550-anti-VGAT-C and VGLUT1 in the CA1 region (***F–F″***). Scale bars: 1 mm (***A***), 250 μm (***B***), 10 μm (***D***), 30 μm (***F***, also valid for ***C***, ***E***).

of striatal and hippocampal neurons were analyzed by whole cell recordings in voltage clamp mode. Evoked synaptic responses recorded from labeled striatal neurons were exclusively of IPSC type whereas hippocampal neurons staying unlabeled after antibody treatment always exhibited EPSCs. Miniature IPSC amplitudes, their frequency and the readily releasable pool remained unchanged in Oyster550 anti-VGAT-C labeled cells, whereas the evoked IPSC charge was reduced by 46% relative to unlabeled neurons (supplemental Fig. 5, available at www.jneurosci.org as supplemental material). Anti-VGAT-C treated neurons showed a slight, but nonsignificant reduction in vesicular release probability.

In vivo labeling of GABAergic synapses

Our above experiments suggest that anti-VGAT-C may be a versatile tool to visualize GABAergic terminals also *in vivo*. Therefore, Oyster550-anti-VGAT-C was stereotaxically injected into the CA1 subfield of the hippocampus of adult mice. Bright red immunolabeling reminiscent of the laminar distribution of GABAergic synapses was evident in the injected hemisphere 48 h later (Fig. 4*A*,*B*), with labeled structures exhibiting coincident immunoreactivities for VGAT-N (Fig. 4*C*), GAD (Fig. 4*D*) and synaptophysin (Fig. 4*E*). High-resolution images revealed anti-VGAT-C immunoreactivity surrounding (rather than overlapping) GAD-immunopositive structures (Fig. 4*D*). *In vivo* labeling and VGLUT1 immunostaining produced distribution patterns complementary with that of indirect VGLUT1 localization (Fig. 4*F*) underscoring the specificity of anti-VGAT-C immunoreactivity. We conclude that fluorochromated antibodies specific for the C-terminal of VGAT can also be used to label GABAergic terminals in live animals.

Discussion

Here, we show that the C terminus of VGAT localizes to the SV lumen resulting in an uneven number of transmembrane domains. We also demonstrate that antibodies directed against this domain recognize VGAT in intact neurons and are sequestered by endocytosis without major long-term perturbation of synaptic functions, making these immunoreagents versatile tools to identify release sites of GABA and glycine and to study the kinetics of SV recycling in active synapses.

Our knowledge about the topology of VNTs is largely based on computer predictions that often lack experimental confirmation. The TMHMM algorithm predicted a VGAT transmembrane topology which shows major differences compared with previous models (McIntire et al., 1997). In contrast to the model proposed by McIntire et al. (1997), which agrees with most algorithms predicting transmembrane topologies, the AA 243–263 region is classified by the TMHMM algorithm as part of the first cytoplasmic loop rather than a transmembrane domain. Consequently, VGAT exhibits an uneven number of transmembrane domains whose orientation downstream from serine 242 is inversed with the C-terminal 14–16 residues being localized intraluminally instead of being exposed on the outer SV surface. Accordingly, the N and C-terminal and first luminal domains recognized by anti-VGAT-N, anti-VGAT-C and anti-VGAT-lum1, respectively, were differentially sensitive to pronase treatment of isolated SVs. Our proteolytic assays and mass spectrometry do not provide conclusive support for the exact membrane topology of VGAT. Nevertheless, these results unequivocally confirm that the entire N terminus and the loop containing AA 408–415 face the cytoplasm while both epitopes recognized by anti-VGAT-C and anti-VGAT-lum1 are localized in the lumen of SVs.

The major pronase-resistant C-terminal VGAT fragment migrated as ~10–15 kDa protein. This does not correspond to the expected ~3–4 kDa size of the fragment comprising the luminal C terminus and the last transmembrane domain which was only visible as a weaker signal. Apparently, the small size of the last putative cytoplasmic loop (5–14 AA, depending on the prediction algorithm) renders it partially resistant to proteolytic cleavage, as also reported for synaptogyrin (Stenius et al., 1995). The larger fragment probably represents the C terminus together with the preceding cytoplasmic and luminal loops and 3 transmembrane domains with a cumulative molecular weight of 10–11 kDa. In contrast, the C termini of VGLUT1, VGLUT2 and VAChT were completely degraded confirming the cytoplasmic localization of these protein epitopes. Thus, VGAT exhibits an exceptional transmembrane topology compared with other known VNTs.

VGAT is the only member of the SLC32 family with no other close mammalian relatives identified so far. Our observations underline the evolutionary distance between VGAT and other known VNTs, which belong to the SLC17 (VGLUT 1–3) or the SLC18 family (VMAT1, 2 and VAChT) (Gasnier, 2004). These latter transporter families are homologous to bacterial toxin/drug extruders (Chaudhry et al., 2008b) while VGAT is not. VGAT even shows significant structural differences when compared with other functionally related membrane located GABA transporters (GAT-1, 2, 3 and BGT-1; (Alexander et al., 2007). The refined VGAT topology with an uneven number of transmembrane domains suggests a closer relationship between VGAT and amino acid permeases in plants which share sequence homology (Wipf et al., 2002) and a similar transmembrane topology with a cytoplasmic localization of the N terminus and a C terminus residing on the outer surface of the plasmalemma (Chang and Bush, 1997). The transmembrane topology for VGAT may also implicate differences in its functional regulation compared with other VNTs whose cytosolic C termini are accessible for other regulatory proteins potentially modulating their function; e.g., endophilin regulation of VGLUT1 recycling (Voglmaier et al., 2006).

Short and transient exposure of live neurons to anti-VGAT-C is sufficient for antibody binding and internalization. Labeling is highly selective for GABAergic neurons indicating that anti-VGAT-C endocytosis is mediated by specific epitope binding and not by unspecific fluid phase uptake. Fluorochromated anti-VGAT-C exhibited a remarkable penetration *in vivo*. In a subset of synapses, anti-VGAT-C labeling closely surrounded, though did not entirely overlap, GAD immunoreactivity. This may be due to a sterical competition of internalized and perfusion-fixed anti-VGAT-C and subsequently applied anti-GAD. Interestingly, antibody uptake led to a 46% reduction of the overall evoked IPSC amplitude and slightly but not significantly reduced SV release probability. The individual miniature fusion events, their frequency and the readily releasable vesicle pool remained unchanged indicating that the presence of luminal anti-VGAT-C can lead to subsequent reduction of the efficiency of SV release but does not affect the translocation of GABA into SVs.

Understanding the precise spatial localization of the VGAT C terminus to the SV lumen is vital for exploiting the potential of our approach to live cell imaging and physiology models of inhibitory neurotransmission. Our confocal imaging studies present the possibility of using VGAT as a novel biomarker in studies aimed at elucidating organizing principles of inhibitory synapses. Combined use of *in vivo* labeling and tracer ligands holds promise for revealing novel synaptic circuitries and refined innervation patterns in the brain. Moreover, *in vivo* labeling of functionally intact and electrophysiologically active GABAergic terminals will yield a new dimension of understanding key features of inhibitory neurotransmission, and their perturbations in neuropathological conditions.

References

Alexander SP, Mathie A, Peters JA (2007) Guide to receptors and channels (GRAC), 2nd edition (2007 Revision). Br J Pharmacol 150:S1–S168.

Boulland J L, Jenstad M, Boekel AJ, Wouterlood FG, Edwards RH, Storm-Mathisen J, Chaudhry FA (2008) Vesicular glutamate and GABA transporters sort to distinct sets of vesicles in a population of presynaptic terminals. Cereb Cortex. Advance online publication. Retrieved May 22, 2008. doi:10.1093/cercor/bhn077

Chang HC, Bush DR (1997) Topology of NAT2, a prototypical example of a new family of amino acid transporters. J Biol Chem 272:30552–30557.

Chaudhry FA, Reimer RJ, Bellocchio EE, Danbolt NC, Osen KK, Edwards RH, Storm-Mathisen J (1998) The vesicular GABA transporter, VGAT, localizes to synaptic vesicles in sets of glycinergic as well as GABAergic neurons. J Neurosci 18:9733–9750.

Chaudhry FA, Boulland JL, Jenstad M, Bredahl MK, Edwards RH (2008a) Pharmacology of neurotransmitter transport into secretory vesicles. Handb Exp Pharmacol 184:77–106.

Chaudhry FA, Edwards RH, Fonnum F (2008b) Vesicular neurotransmitter transporters as targets for endogenous and exogenous toxic substances. Annu Rev Pharmacol Toxicol 48:277–301.

Erickson JD, Weihe E, Schäfer MK, Neale E, Williamson L, Bonner TI, Tao-Cheng JH, Eiden LE (1996a) The VAChT/ChAT "cholinergic gene locus": new aspects of genetic and vesicular regulation of cholinergic function. Prog Brain Res 109:69–82.

Erickson JD, Schafer MK, Bonner TI, Eiden LE, Weihe E (1996b) Distinct pharmacological properties and distribution in neurons and endocrine cells of two isoforms of the human vesicular monoamine transporter. Proc Natl Acad Sci U S A 93:5166–5171.

Gasnier B (2000) The loading of neurotransmitters into synaptic vesicles. Biochimie 82:327–337.

Gasnier B (2004) The SLC32 transporter, a key protein for the synaptic release of inhibitory amino acids. Pflugers Arch 447:756–759.

Gauthier-Campbell C, Bredt DS, Murphy TH, El-Husseini Ael-D (2004) Regulation of dendritic branching and filopodia formation in hippocampal neurons by specific acylated protein motifs. Mol Biol Cell 15:2205–2217.

Härtig W, Seeger J, Naumann T, Brauer K, Brückner G (1998) Selective in vivo fluorescence labelling of cholinergic neurons containing $p75^{NTR}$ in the rat basal forebrain. Brain Res 808:155–165.

Jahn R (1999) Recycling of synaptic vesicle membrane within nerve terminals. Brain Res Bull 50:313–314.

Klingauf J, Kavalali ET, Tsien RW (1998) Kinetics and regulation of fast endocytosis at hippocampal synapses. Nature 394:581–585.

Kraszewski K, Mundigl O, Daniell L, Verderio C, Matteoli M, De Camilli P (1995) Synaptic vesicle dynamics in living cultured hippocampal neurons visualized with CY3-conjugated antibodies directed against the lumenal domain of synaptotagmin. J Neurosci 15:4328–4342.

Laemmli UK (1970) Cleavage of structural proteins during the assembly of the head of bacteriophage T4. Nature 227:680–685.

Liu Y, Edwards RH (1997) The role of vesicular transport proteins in synaptic transmission and neural degeneration. Annu Rev Neurosci 20:125–156.

Masson J, Sagné C, Hamon M, El Mestikawy S (1999) Neurotransmitter transporters in the central nervous system. Pharmacol Rev 51:439–464.

McIntire SL, Reimer RJ, Schuske K, Edwards RH, Jorgensen EM (1997) Identification and characterization of the vesicular GABA transporter. Nature 389:870–876.

Nagy A, Baker RR, Morris SJ, Whittaker VP (1976) The preparation and characterization of synaptic vesicles of high purity. Brain Res 109:285–309.

Perin MS, Brose N, Jahn R, Südhof TC (1991) Domain structure of synaptotagmin (p65). J Biol Chem 266:623–629.

Pyott SJ, Rosenmund C (2002) The effects of temperature on vesicular supply and release in autaptic cultures of rat and mouse hippocampal neurons. J Physiol 593:523–535.

Schägger H, von Jagow G (1987) Tricine-sodium dodecyl sulfate-polyacrylamide gel electrophoresis for the separation of proteins in the range from 1 to 100 kDa. Anal Biochem 166:368–379.

Schneider WJ, Slaughter CJ, Goldstein JL, Anderson RG, Capra JD, Brown MS (1983) Use of antipeptide antibodies to demonstrate external orientation of the NH2-terminus of the low density lipoprotein receptor in the plasma membrane of fibroblasts. J Cell Biol 97:1635–1640.

Schoch S, Gundelfinger ED (2006) Molecular organization of the presynaptic active zone. Cell Tissue Res 326:379–391.

Siegemund T, Paulke BR, Schmiedel H, Bordag N, Hoffmann A, Harkany T, Tanila H, Kacza J, Härtig W (2006) Thioflavins released from nanoparticles target fibrillar amyloid beta in the hippocampus of APP/PS1 transgenic mice. Int J Dev Neurosci 24:195–201.

Stenius K, Janz R, Südhof TC, Jahn R (1995) Structure of synaptogyrin (p29) defines novel synaptic vesicle protein. J Cell Biol 131:1801–1809.

Sudhof TC (2004) The synaptic vesicle cycle. Annu Rev Neurosci 27:509–547.

Takamori S (2006) VGLUTs: 'exciting' times for glutamatergic research? Neurosci Res 55:343–351.

Takamori S, Riedel D, Jahn R (2000) Immunoisolation of GABA-specific synaptic vesicles defines a functionally distinct subset of synaptic vesicles. J Neurosci 20:4904–4911.

Towbin H, Staehelin T, Gordon J (1979) Electrophoretic transfer of proteins from polyacrylamide gels to nitrocellulose sheets: procedure and some applications. Proc Natl Acad Sci U S A 76:4350–4354.

Voglmaier SM, Kam K, Yang H, Fortin DL, Hua Z, Nicoll RA, Edwards RH (2006) Distinct endocytic pathways control the rate and extent of synaptic vesicle protein recycling. Neuron 51:71–84.

Wipf D, Ludewig U, Tegeder M, Rentsch D, Koch W, Frommer WB (2002) Conservation of amino acid transporters in fungi, plants and animals. Trends Biochem Sci 27:139–147.

European Journal of Neuroscience, Vol. 27, pp. 691–701, 2008 doi:10.1111/j.1460-9568.2008.06047.x

Reduction in memory in passive avoidance learning, exploratory behaviour and synaptic plasticity in mice with a spontaneous deletion in the ubiquitin C-terminal hydrolase L1 gene

Mikako Sakurai,[1,*] Masayuki Sekiguchi,[1,2,*] Ko Zushida,[1,2] Kazuyuki Yamada,[3] Satoshi Nagamine,[1] Tomohiro Kabuta[1] and Keiji Wada[1,2]

[1]Department of Degenerative Neurological Diseases, National Institute of Neuroscience, National Center of Neurology and Psychiatry, 4-1-1 Ogawahigashi, Kodaira, Tokyo 187–8502, Japan

[2]CREST, Japan Science and Technology Agency, Kawaguchi, Saitama 322–0012, Japan

[3]Support Unit for Animal Experiments, Brain Science Institute, RIKEN, 2–1 Hirosawa, Wako, Saitama 351–0198, Japan

Keywords: Alzheimer's disease, CREB, hippocampus, LTP, transcription

Abstract

Overexpression of ubiquitin C-terminal hydrolase L1 (UCH-L1) in mice rescues amyloid β-protein-induced decreases in synaptic plasticity and memory. However, the physiological role of UCH-L1 in the brain is not fully understood. In the present study, we investigated the role of UCH-L1 in the brain by utilizing gracile axonal dystrophy (*gad*) mice with a spontaneous deletion in the gene *Uch-l1* as a loss-of-function model. Although *gad* mice exhibit motor paresis beginning at ~12 weeks of age, it is possible to analyse their brain phenotypes at a younger age when no motor paresis is evident. Maintenance of memory in a passive avoidance test and exploratory behaviour in an open field test were reduced in 6-week-old *gad* mice. The maintenance of theta-burst stimulation-induced long-term potentiation (LTP) of field synaptic responses from Schaffer collaterals to CA1 pyramidal cells in hippocampal slices was also impaired in *gad* mice. The LTP in *gad* mice was insensitive to actinomycin D, suggesting that a transcription-dependent component of the LTP is impaired. Phosphorylation of cyclic AMP response element binding protein (CREB) in the CA1 region of hippocampal slices from *gad* mice occurred earlier than in the slices from wild-type mice and was transient, suggesting that CREB phosphorylation is altered in *gad* mice. These results suggest that memory in passive avoidance learning, exploratory behaviour and hippocampal CA1 LTP are reduced in *gad* mice. We propose that UCH-L1-mediated maintenance of the temporal integrity and persistence of CREB phosphorylation underlies these impairments.

Introduction

Ubiquitin C-terminal hydrolase L1 (UCH-L1) is a deubiquitinating enzyme (Wilkinson *et al.*, 1989) that is exclusively expressed in the brain and testis, and its expression is neuron-specific in the brain (Wilkinson *et al.*, 1989). Several lines of evidence suggest that UCH-L1 is involved in idiopathic Alzheimer's disease (AD) and Parkinson's disease (PD): (i) UCH-L1 is down-regulated in idiopathic AD and PD (Choi *et al.*, 2004), and in an AD model mouse (Gong *et al.*, 2006); and (ii) UCH-L1 is oxidatively modified in AD brains (Castegna *et al.*, 2002). Substitution of tyrosine for serine at codon 18 (S18Y polymorphism) in the *Uch-l1* gene exerts a protective effect against sporadic AD (Xue & Jia, 2006) and PD (Maraganore *et al.*, 1999). Furthermore, substitution of methionine for isoleucine at codon 93 (I93M mutation) reduces hydrolase activity of UCH-L1 and is linked to a rare autosomal dominant form of familial PD in a German family (Leroy *et al.*, 1998). Although these findings point to a role for UCH-L1 in AD and PD, the physiological role of UCH-L1 in the normal mammalian brain is not fully understood.

UCH-L1 has multiple functions *in vitro*. UCH-L1 removes small adducts or unfolded polypeptides from ubiquitin's C-terminus via hydrolysis (Larsen *et al.*, 1998). In addition, UCH-L1 has ubiquitin-ligase activity on α-synuclein-ubiquitin conjugates (Liu *et al.*, 2002). Apart from enzymatic activity, UCH-L1 acts as a stabilizer of monoubiquitin (Osaka *et al.*, 2003). UCH-L1 is thought to be a therapeutic target for AD; specifically, overexpression of UCH-L1 rescues amyloid β-protein (Aβ)-induced decreases in synaptic plasticity and contextual memory in mice (Gong *et al.*, 2006). Pharmacological suppression of UCH-L1 hydrolase activity (by 70%) is associated with impairment of synaptic transmission, tetanus-induced long-term potentiation (LTP) in the hippocampal CA1 field, and contextual fear memory in mice (Gong *et al.*, 2006). The nonmammalian Aplysia UCH has been identified as an immediate–early gene essential for long-term synaptic facilitation in the nervous system (Hedge *et al.*, 1997).

The aim of the present study was to further characterize the role of UCH-L1 in the mammalian brain. To this end, we utilized the UCH-L1-deficient *gracile axonal dystrophy* (*gad*) mouse, which is a spontaneous mutant with an in-frame deletion in exons 7 and 8 of *Uch-l1* (Saigoh *et al.*, 1999). Expression of the UCH-L1 protein is

Correspondence: Dr Keiji Wada, [1]Department of Degenerative Neurological Diseases, as above.
E-mail: wada@ncnp.go.jp

*M. Sakurai and M. Sekiguchi contributed equally to this study

Received 12 July 2007, revised 10 December 2007, accepted 12 December 2007

undetectable in the central nervous system of *gad* mice (Osaka *et al.*, 2003). In addition, recent analysis in our laboratory suggests that truncated products from the mutant *Uch-l1* are not detected in the *gad* mouse brain (T. Kabuta, unpublished observation). Although *gad* mice exhibit motor paresis beginning at ~ 12 weeks of age due to axonal degeneration of spinal cord neurons and subsequent degeneration of the spinocerebellar tract (Kikuchi *et al.*, 1990), it is possible to analyse the brain phenotypes of *gad* mice at younger ages when no motor paresis is evident. We found that memory in passive avoidance learning, exploratory behaviour and hippocampal synaptic plasticity are reduced in young *gad* mice (6 weeks of age).

Materials and Methods

Animals

Gad mice were bred at the Experimental Animal Center of the National Institute of Neuroscience, National Center of Neurology and Psychiatry, Tokyo. The original genetic background of *gad* mice was a hybrid of the CBA and RFM strains (Kikuchi *et al.*, 1990). However, *gad* mice were backcrossed to C57BL/6J strain mice 6–18 times before use in the present study. Six-week-old male *gad* mice and wild-type mice generated from heterozygous *gad* mating pairs were used for the experiments. Genotyping was carried out using PCR with the following three primers:

F1, 5′- agcttggagcctgtggtttcaactc-3′;
R1, 5′-tggcagcatcctgaaaaggagaggtg-3′;
R2, 5′-tacagatggccgtccacgttgttga-3′

The reaction conditions were 35 cycles of 94 °C for 20 s, 60 °C for 30 s and 72 °C for 60 s. The wild-type allele produced an 891-bp PCR product, and the *gad* allele produced a 446-bp PCR product. Three to five mice were housed per cage under controlled temperature (25 ± 1 °C) and lighting (12-h light–dark cycle) conditions and provided with food and water *ad libitum*. The experiments were performed in strict accordance with the National Institute of Neuroscience's regulations for animal experimentation, and were approved by the Animal Investigation Committee of the Institute.

Histology

Hematoxylin and eosin (H&E) staining was performed as reported (Kikuchi *et al.*, 1990). For immunohistochemistry, 4-μm-thick paraffin sections were de-paraffinized and pretreated in a microwave oven with 10 mM citrate–NaOH buffer (pH 6.0). After blocking with phosphate-buffered saline containing 1% heat-inactivated normal goat serum and 0.1% [(v/v)] Triton X-100, slides were incubated with an anti-Aβ monoclonal antibody (clone 4G8, 1 : 100 dilution; Signet Laboratories, Dedham, MA, USA) or an antisynaptophysin monoclonal antibody (MAB5258, 1 : 500 dilution; Chemicon, Temecula, CA, USA) and then with Envision+horseradish peroxidase–labelled anti-mouse IgG (DakoCytomation Inc., Carpinteria, CA, USA). Chromogenic detection was performed using the DAB Substrate kit (DakoCytomation Inc.). Sections were examined with a BX51 microscope (Olympus).

Behavioural tests

One-trial passive avoidance tests were performed as described (Yamada *et al.*, 2003). Briefly, a single mouse was introduced into a light compartment of a light–dark box (Muromachi-kikai, Tokyo, Japan). During habituation, mice were allowed to freely explore the box for 5 min with the sliding door between the light and dark compartments open; after that, the mice were returned to their home cage. For conditioning, which was carried out 2 h after habituation, the mice were introduced into the light compartment, the sliding door was closed when both hindlimbs had entered into the dark box, and an electrical footshock was delivered via the floor grid in the dark compartment (300 μA, 3 s duration, using a shock generator–scrambler; Muromachi-kikai). The mice were left in the light–dark box for 5 min and then returned to their home cage. Tests were carried out 2 or 24 h after the conditioning by re-introducing the mice into the light compartment of the light–dark box. The latency time for mice to enter the dark compartment was measured (light–dark latency, with a 5 min cut-off). The tests at 2 and 24 h postconditioning were carried out using different groups of mice.

The pain sensitivity of mice was tested as described (Yamada *et al.*, 2003). Briefly, a series of footshocks of ascending (20, 40, 60, 80, 100 and 130 μA, 1 s duration) and descending (130, 100, 80, 60, 40 and 20 μA, 1 s duration) current were serially delivered to the mice via the floor grid. The input current that induced hindlimb withdraw was recorded. The interfootshock interval was 15 s. This trial was performed six times, and the data were averaged.

Open field tests were performed as we described (Zushida *et al.*, 2007). Briefly, the test was carried out in an arena (a 50 × 50 cm white field surrounded by a 40-cm-high white wall, illuminated with 80 lx) placed in a soundproof box. Mice were placed at the periphery of the arena, and for 5 min the behaviour of the mice was recorded using a digital video camera linked to a computer. Locomotor activity was calculated from this record by Image OF (O'Hara & Co., Ltd, Tokyo, Japan), modified software based on the public domain NIH Image program. Rearing was manually counted.

The light–dark box test was performed as described (Yamada *et al.*, 2002). Briefly, mice were placed into the dark compartment of the light–dark box and were allowed to explore both sides of the light–dark box for 5 min. During these 5 min, three parameters were measured: latency to enter the light compartment, number of entries into the light compartment, and duration in the light compartment.

Electrophysiology

Each 6-week-old male mouse was anaesthetized with halothane, and the brain was quickly removed. Preparation of hippocampal slices for electrophysiology was carried out as reported (Takamatsu *et al.*, 2005; Zushida *et al.*, 2007). Briefly, the hippocampus was isolated from the brain, and transverse slices (400 μm thick) were prepared using a Vibratome 3000 microtome (Vibratome Company, St Louis, MO, USA) in a sucrose-based cutting solution (in mM: sucrose, 234; KCl, 25; NaH_2PO_4, 1.25; $MgSO_4$, 10; $NaHCO_3$, 26; glucose, 11; and $CaCl_2$, 0.5). The slices were maintained at room temperature in artificial cerebrospinal fluid (ACSF; in mM: NaCl, 125; KCl, 4.4; $MgSO_4$, 1.5; NaH_2PO_4, 1.0; $NaHCO_3$, 26; glucose, 10; and $CaCl_2$, 2.5; pH 7.4, 290–300 mOsm/L) continuously bubbled with 95% O_2 and 5% CO_2. A slice was then transferred to the recording chamber and was continuously superfused at 3 mL/min with ACSF maintained at 28–32 °C.

Extracellular field recordings were carried out as reported (Takamatsu *et al.*, 2005). Briefly, field excitatory postsynaptic potentials (fEPSPs) were recorded from CA1 stratum radiatum of the hippocampus using a glass micropipette (1–2 MΩ) filled with ACSF. The electrical signals were amplified using a MultiClamp 700B amplifier (Axon Instruments, Foster City, CA, USA), filtered at 10 kHz, digitized at 10 kHz and acquired with Clampex (ver. 9.2). A bipolar stainless steel stimulating electrode was placed in stratum radiatum at the border between CA2 and CA3 to stimulate the Schaffer collateral pathway. The pulse intensity was adjusted to give 40% of the maximum amplitude in all experiments. Stimulation was carried out in

constant current mode (100 μs duration). The fEPSPs for which the 40% amplitude was > 1 mV were used for data analysis. The strength of synaptic transmission was determined by measuring the rising phase (20–60%) of the fEPSP slope. The average fEPSP slope during the 10 min prior to LTP induction was taken as the baseline, and all values were normalized to this baseline. The baseline stimulation frequency was 0.033 Hz. LTP was induced by applying theta-burst stimulation (TBS; 15 bursts of four pulses at 100 Hz, delivered at an interburst interval of 200 ms) or tetanic stimulation (100 Hz, 1 s, three times with a 20 s interval). Paired-pulse facilitation was induced by delivering two consecutive pulses with a 20-, 50-, 100-, 200- or 400-ms interpulse interval.

Somatic whole-cell patch-clamp recordings were made with a MultiClamp 700B amplifier (Zushida *et al.*, 2007). Pyramidal-shaped neurons in the CA1 pyramidal layer visually identified with differential contrast video microscopy (Hamamatsu Photonics, Hamamatsu, Japan) on an upright microscope (Axioscope, Zeiss, Oberkochen, Germany) were selected for recording. The patch electrodes were 6–10 MΩ when filled with a solution containing (in mM): K gluconate, 132; KCl, 3; HEPES, 10; EGTA, 0.5; $MgCl_2$, 1; sodium phosphocreatine, 12; ATP·Mg, 3; and GTP, 0.5 (pH 7.4 with KOH, 285–290 mOsm/L). We used this solution when measuring membrane potential and input resistance. The input resistance was calculated by injecting a square current pulse (−10 pA) in current-clamp mode. For comparison of synaptic currents at −70 and +40 mV, an internal solution containing (in mM): CsOH, 105; CsCl, 30; HEPES, 10; EGTA, 0.5; $MgCl_2$, 1; sodium phosphocreatine, 12; ATP·Mg, 3; and GTP, 0.5 (pH 7.3 with gluconic acid, 295 mOsm/L) was used. The signal was digitized at one point per 50 μs and stored using Clampex. The resting membrane potential of the cells used in the analysis ranged from −57 to −67 mV, and the series resistance was 3–20 MΩ. Synaptic responses were elicited by electrical stimulation as described for extracellular recording. The pulse intensity was adjusted to elicit excitatory postsynaptic potentials (EPSPs) 40% of the amplitude required for action potential generation in current-clamp mode.

All chemicals and drugs used for electrophysiology were purchased from Sigma with the exception of actinomycin D, which was obtained from Wako Pure Chemicals (Tokyo, Japan). Actinomycin D was dissolved in dimethylsulfoxide at 40 mM, added to ACSF just prior to application at 40 μM, and bath-applied with perfusion. Therefore, the final dimethylsulfoxide concentration was 0.1%.

Western blotting

For analysis of Aβ, the hippocampus was isolated from the brain and snap-frozen in liquid nitrogen. The tissue was homogenized in ice-cold buffer (Tris-HCl, 50 mM; NaCl, 150 mM; EDTA, 5 mM; and Triton X-100, 1%; pH 7.5) containing proteinase inhibitors (Complete, EDTA-free; Roche Applied Science, Indianapolis, IN, USA) and phosphatase inhibitors (Halt phosphatase inhibitor cocktail; Pierce, Rockford, IL, USA), and the homogenate was subjected to SDS-PAGE. Western blotting was carried out as we reported (Kabuta *et al.*, 2006) using anti-Aβ (clone 4G8; Signet Laboratories), anti-UCH-L1 (UltraClone Ltd, UK) and anti-β-actin (Sigma) antibodies. Briefly, immunoreactive signals were visualized with SuperSignal West Femto maximum sensitivity substrate (Pierce) or SuperSignal West Dura extended duration substrate (Pierce) and detected with a chemiluminescence imaging system (FluorChem; Alpha Innotech, San Leandro, CA, USA). Human Aβ 1–42 from Peptide Institute, Inc., Osaka, Japan served as the positive control.

Following extracellular recording, hippocampal slices were retrieved for Western blotting. The dentate gyrus and CA3 region of the slices were cut off, and the remaining CA1 region was snap-frozen in liquid nitrogen. Tissue samples from each slice were homogenized in the same buffer as used for the Aβ analysis, and the homogenate was subjected to SDS-PAGE. The antibodies used were anti-phospho-CREB (serine 133), anti-CREB (Cell Signalling Technology, Inc., Danvers, MA, USA), anti-cAMP-dependent protein kinase (protein kinase A; PKA) regulatory subunit RIα and RIIα (BD Biosciences, San Jose, CA, USA), anti-UCH-L1 (UltraClone Ltd) and anti-β-actin (Sigma). Immunoreactive signals were visualized as described for the Aβ analysis. The signal intensity was quantified by densitometry using FluoChem software (Alpha Innotech).

Data and statistical analysis

Numerical data are expressed as the mean ± SEM. The two-tailed Student's *t*-test was used for comparison between wild-type mice and *gad* mice. Repeated-measures one-way ANOVA was used to analyse whether footshock and exposure to an open field arena had significant effects within a genotype in passive avoidance and open field tests, respectively. ANOVA with the Bonferroni–Dunn test was used to compare the three data groups in the pCREB analysis.

Results

Structural abnormalities were not detected in the cerebrum and hippocampus of young gad mice

Before behavioural analysis, we first examined whether there were any histological abnormalities in the cerebral cortex and hippocampus of 6-week-old *gad* mice. It has been reported that the thalamus is not impaired in *gad* mice (Kikuchi *et al.*, 1990), but there is no report on the cortex and limbic system. Figure 1A–D shows H&E staining of coronal brain sections (at bregma level −1.7 mm) from a wild-type mouse (Fig. 1A and C) and *gad* mouse (Fig. 1B and D; 6 weeks of age). We could not detect any visible abnormalities, such as atrophy or lack of cells, in the hippocampus or cortex of *gad* mice ($n = 2$). One anatomical characteristic of *gad* mice is spheroid structures in the medulla and spinal cord that are thought to be degenerating axons (Kikuchi *et al.*, 1990). We did not find this aberration in the hippocampus or cortex of *gad* mice (Fig. 1A–D). We also examined other brain regions in sections cut at bregma levels 2.5, 1.0, −3.0 and −6.0 mm, and no outstanding abnormalities were evident in the *gad* mice (data not shown). In addition, we carried out immunohistochemical staining using antisynaptophysin. This antibody stains presynaptic sites and thus the staining pattern would be expected to be different in *gad* mice if there was noticeable axonal degeneration. Typical punctate synaptophysin staining was obtained in both wild-type (Fig. 1E and G) and *gad* (Fig. 1F and H) mice. We could not detect any visible differences in the staining of the hippocampus between wild-type and *gad* mice. These results suggest that structural impairment of the brain at a macroanatomical level is not evident in 6-week-old *gad* mice.

Axonal degeneration promotes accumulation of Aβ in the medulla and spinal cord of *gad* mice (Ichihara *et al.*, 1995). Consistent with the lack of spheroid structures in the cortex and hippocampus, we did not find abnormal accumulation of Aβ in these brain regions in *gad* mice up to 12 weeks of age (immunohistochemical analysis using an antibody to Aβ; data not shown). Furthermore, we examined nonfibrillar Aβ by Western blotting. We could not detect any significant bands in the samples from wild-type and *gad* mouse hippocampi when blotting with anti-Aβ (Fig. 1I, upper panel). Authentic human Aβ (the right two lanes, a positive control) blotted

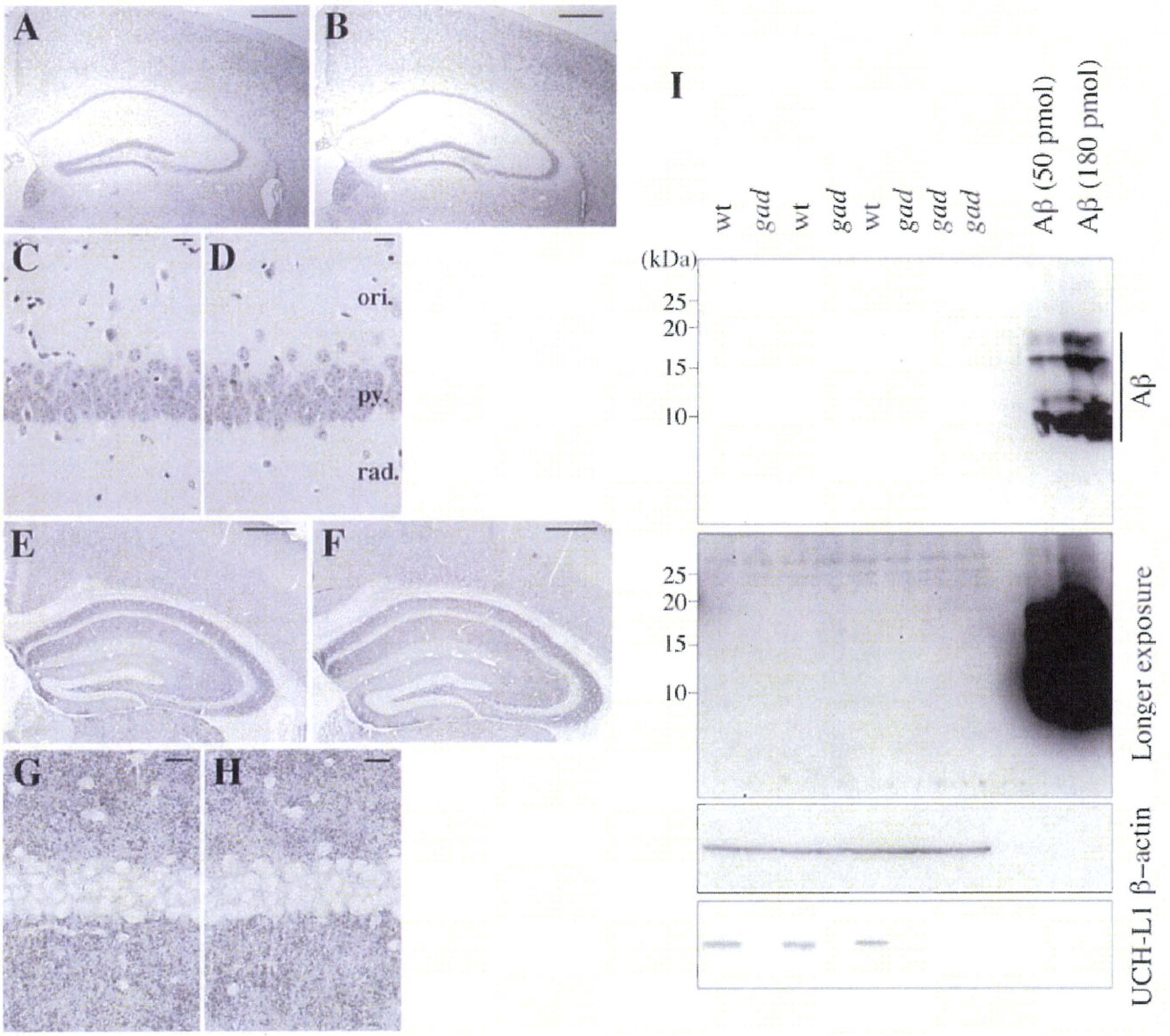

FIG. 1. Six-week-old *gad* mice have normal brain histology. (A–D) H&E staining of coronal brain sections from (A and C) a 6-week-old wild-type (wt) mouse and (B and D) a 6-week-old *gad* mouse. (C and D) A higher magnification of the hippocampal CA1 field. ori., stratum oriens; py., pyramidal cell layer; rad., stratum radiatum. (E–H) Synaptophysin immunohistochemistry in coronal brain sections from a six-week-old wt mouse (E and G) and a six-week-old *gad* mouse (F and H). (G and H) A higher magnification of the hippocampal CA1 field. (I) Western blotting of samples prepared from the hippocampi of three wt and five *gad* mice. Antibodies against Aβ, β-actin and UCH-L1 were used. Authentic Aβ was used as a positive control. A short exposure is shown in the upper panel; a longer exposure is shown below. Molecular size markers (kDa) are shown on the left. Scale bars, 500 μm (A, B, E and F), 20 μm (C, D, G and H).

densely on the same membrane. After a longer exposure (Fig. 1I) we could detect certain bands, but there was no band that was significantly increased in *gad* mice compared with wild-type mice. Blots using anti β-actin and anti-UCH-L1 were carried out to confirm the sample load and genotype, respectively (Fig. 1I).

Lack of UCH-L1 in mice impaired memory maintenance in the passive avoidance test and exploratory behaviour for a novel environment

Next, we examined whether lack of UCH-L1 had a detectable impact on mouse behaviour. For this purpose, we carried out one-trial passive avoidance tests. Figure 2A shows the performance of wild-type and *gad* mice in this test. After habituation to the light–dark box, mice were conditioned with an electrical footshock when they entered the dark compartment. We then tested their ability to avoid the dark compartment 24 h after the conditioning footshock. The footshock significantly prolonged the light–dark latency in wild-type mice (comparison of the conditioning and test sessions $P = 0.003$, $F = 14.6$, $n = 12$; repeated-measures ANOVA). In contrast, the light–dark latency was not significantly affected in *gad* mice (comparison of the conditioning and test sessions using repeated-measures ANOVA, $P = 0.2437$, $F = 1.556$, $n = 10$), suggesting that memory function, as assessed by this test, is impaired in *gad* mice. In

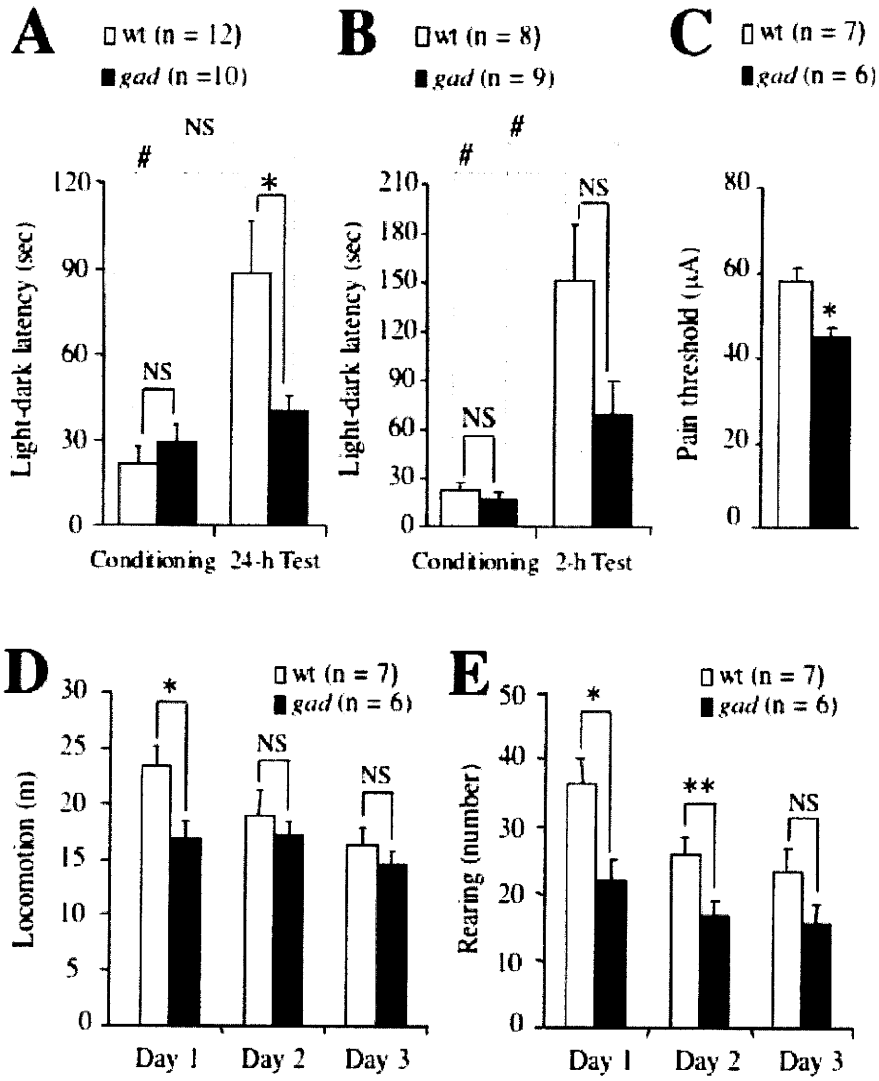

FIG. 2. Impairment of memory maintenance and exploratory behaviour in *gad* mice. (A and B) Light–dark latency of mice in a one-trial passive avoidance test. After habituation to a light–dark box, mice were conditioned with an electrical footshock when they entered the dark compartment (Conditioning). At (A) 24 h or (B) 2 h after the footshock, the mice were reintroduced into the light–dark box and the time for mice to enter the dark compartment (light–dark latency) was measured (Test). $^{*}P = 0.028$; NS, not significant; two-tailed Student's *t*-test (solid lines). $^{\#}P < 0.020$; NS, not significant, repeated-measures one-way ANOVA (dotted lines). (C) Pain sensitivity of the mice was measured by applying a series of electrical footshocks. $^{*}P = 0.002$, two-tailed Student's *t*-test. (D) Locomotor activity of wild-type and *gad* mice in an open field arena. The mice were introduced into the arena for the first time on day 1. $^{*}P = 0.023$, two-tailed Student's *t*-test. (E) Rearing frequency of wild-type and *gad* mice in an open field arena. $^{*}P = 0.014$, $^{**}P = 0.021$; two-tailed Student's *t*-test.

addition, the light–dark latency in the 24-h test session differed significantly between the wild-type and *gad* mice ($P = 0.028$; two-tailed Student's *t*-test). We next conducted a test session 2 h after conditioning to test whether learning ability was impaired in *gad* mice shortly after conditioning. In the test 2 h after conditioning (Fig. 2B), the footshock had a significant effect on the light–dark latency in both wild-type and *gad* mice ($P = 0.0147$, $F = 10.356$, $n = 8$ for wild-type mice; $P = 0.0199$, $F = 8.407$, $n = 9$ for *gad* mice; repeated-measures ANOVA). The average latency in the 2-h test session did not differ significantly between the wild-type and *gad* mice ($P = 0.074$; two-tailed Student's *t*-test). These results suggest that *gad* mice are able to learn but maintenance of memory is reduced. Because the pain sensitivity of *gad* mice was greater than that of wild-type mice (Fig. 2C; $P = 0.002$ with two-tailed Student's *t*-test), the footshock used for conditioning was indeed an aversive stimulus in *gad* mice.

Next, we carried out the open field test. Mice were exposed to an open field arena for the first time on day 1 (Fig. 2D). The wild-type mice explored the novel environment and showed high locomotor activity (Fig. 2D). Locomotor activity was reduced upon re-exposure of wild-type mice to the same arena on days 2 and 3 because they remembered the arena, and thus the novelty was reduced ($P = 0.024$, $F = 12.928$, $n = 7$; repeated-measures ANOVA). In contrast, locomotor activity was not significantly decreased in *gad* mice ($P = 0.392$, $F = 1.030$, $n = 6$; repeated-measures ANOVA). The locomotor activity on day 1 differed significantly between wild-type and *gad* mice ($P = 0.023$; two-tailed Student's *t*-test), but the activity on day 2 or 3 did not ($P = 0.500$ and 0.446 for days 2 and

3, respectively). To determine whether the difference in locomotor activity on day 1 was due to reduced exploratory behaviour in *gad* mice, we measured the frequency of rearing, a typical exploratory behaviour (Lever *et al.*, 2006; Fig. 2E). Similar to locomotor activity, upon re-exposure rearing frequency decreased in wild-type mice ($P = 0.009$, $F = 14.257$, $n = 7$; repeated-measures ANOVA) but not in *gad* mice ($P = 0.131$, $F = 2.503$, $n = 6$; repeated-measures ANOVA). The rearing frequency on days 1 and 2 differed significantly between wild-type and *gad* mice ($P = 0.014$ and 0.021 for days 1 and 2, respectively; two-tailed Student's *t*-test), but the activity on day 3 did not ($P = 0.093$). These results suggest that exploratory behaviour in a novel environment is reduced in *gad* mice.

Although these data apparently suggest that memory in passive avoidance learning and exploratory behaviour are reduced in young *gad* mice, there is a possibility that the anxiety state of *gad* mice is altered. Alterations in the anxiety state can affect memory (Bouton *et al.*, 1990) and the response to novel environments. To measure anxiety, we performed a light–dark box test. In this test, mice usually avoid the light compartment. Therefore, the level of anxiety can be measured as the latency to move into the light compartment and the duration of time in the light compartment (Yamada *et al.*, 2002). Because the passive avoidance test also utilizes these properties, performance in the light–dark test is important for interpreting the results from the passive avoidance test. The time required for the mice to step into the light compartment when introduced into the dark compartment (dark-light latency; Fig. 3A), the time the mice spent in the light compartment (Fig. 3A) and the number of times the mice crossed between compartments (Fig. 3B) did not differ significantly between wild-type and *gad* mice ($P = 0.834$, 0.417 and 0.109, respectively; two-tailed Student's *t*-test). These results suggest that anxiety state, as assessed by this test, was not obviously altered in *gad* mice. Therefore we concluded that the impairments in passive avoidance learning and exploratory behaviour were not due to alterations in the anxiety state.

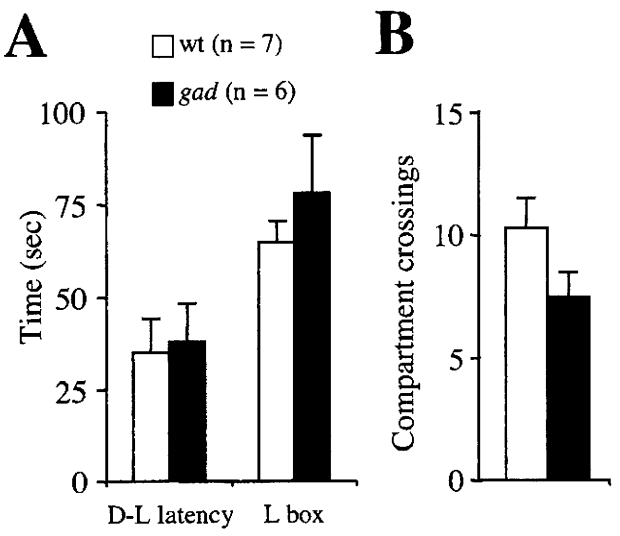

FIG. 3. Wild-type and *gad* mice performed similarly in the light–dark box test. (A) Dark–light (D-L) latency and duration of time in the light compartment (L box). (B) Number of crossings between the two compartments.

Impairment of a transcription-dependent component of LTP in gad mice

We tested whether the lack of UCH-L1 affects neuronal function by measuring LTP at Schaffer collateral synapses onto CA1 pyramidal neurons in hippocampal slice preparations. LTP is believed to be a synaptic mechanism underlying memory and learning (Bliss & Collingridge, 1993). The CA1 synapse was selected because this brain region is involved in spatial memory (Morris *et al.*, 1982) and passive avoidance memory (Bevilaqua *et al.*, 1997; Impey *et al.*, 1998). In wild-type slices, TBS induced robust LTP at CA1 synapses (Fig. 4A), as reported for C57BL/6J mice (Nguyen & Kandel, 1997; Nguyen *et al.*, 2000). In contrast, TBS-induced LTP was attenuated in *gad* mice beginning ~20 min post-TBS (Fig. 4A). At 45 min post-TBS, normalized synaptic responses were significantly greater in wild-type slices (1.87 ± 0.08, $n = 7$) than in *gad* slices (1.36 ± 0.07, $n = 6$; $P = 0.001$, two-tailed Student's *t*-test). Impairment of LTP in *gad* mice depended on the stimulation pattern. Tetanus-induced LTP was identical in wild-type and *gad* mice (Fig. 4B; normalized fEPSP slopes at 45 min post-tetanus: wild-type, 1.81 ± 0.16, $n = 5$; *gad*, 1.86 ± 0.25, $n = 5$).

Stimulus–output curves (Fig. 5A) and paired-pulse facilitation (Fig. 5B) of CA1 synapses were essentially identical in wild-type and *gad* mice. The latter result suggests that a postsynaptic, rather than presynaptic, mechanism is involved in impairment of TBS-induced LTP in *gad* mice. LTP at this synapse is dependent on postsynaptic NMDA receptors (Harris *et al.*, 1984; Larson & Lynch, 1988). Therefore, we tested whether NMDA receptor activity was reduced in *gad* mice using patch-clamp recordings. For this purpose, we recorded Schaffer collateral–CA1 synaptic responses in neurons voltage-clamped to −70 and +40 mV in the presence of picrotoxin (50 μM). The amplitude of the synaptic response recorded at +40 mV at 100 ms poststimulation was normalized to the peak amplitude of the response at −70 mV to estimate the ratio of NMDA-mediated to non-NMDA-mediated currents (Fig. 5D). Because superfusion of the slices with picrotoxin frequently elicited epileptiform activity (data not shown), three to five synaptic responses without epileptiform activity were selected and averaged. The ratio was identical in wild-type and *gad* mice (0.45 ± 0.05, $n = 5$ and 0.43 ± 0.05, $n = 7$ for wild-type and *gad* mice, respectively; two-tailed Student's *t*-test). Therefore, attenuation of synaptic NMDA receptor activity does not account for reduced LTP in *gad* mice. Resting membrane potential and input resistance of CA1 pyramidal neurons did not differ substantially between wild-type and *gad* mice [resting membrane potential, -60.1 ± 0.4 mV for wild-type mice ($n = 20$) and -60.0 ± 0.6 mV for *gad* mice ($n = 20$); input resistance, 163 ± 9.6 for wild-type mice ($n = 16$) and 175 ± 10.8 for *gad* mice ($n = 13$); results obtained from the records using potassium-gluconate pipette solution].

CA1 LTP is composed of early and late temporal phases (Nguyen *et al.*, 1994; Abel *et al.*, 1997; Nguyen & Kandel, 1997). The former is induced mainly by an increase in the number of AMPA-type glutamate receptors at the synapse (reviewed in Malinow & Malenka, 2002) whereas the latter is induced by new protein synthesis from transcription of new mRNA (Nguyen *et al.*, 1994) and/or local protein synthesis from previously expressed mRNA (Bradshaw *et al.*, 2003). Because no obvious changes in the early phase of LTP (up to ~20 min post-TBS) were observed in *gad* mice, we tested whether the late phase is occluded in *gad* mice. For this purpose, we applied actinomycin D, a transcription inhibitor, to the slices and compared suppression of TBS-induced LTP in wild-type and *gad* mice. In wild-type mice, the maintenance of TBS-induced LTP was suppressed by actinomycin D (Fig. 6A). The normalized fEPSP slope at 45 min

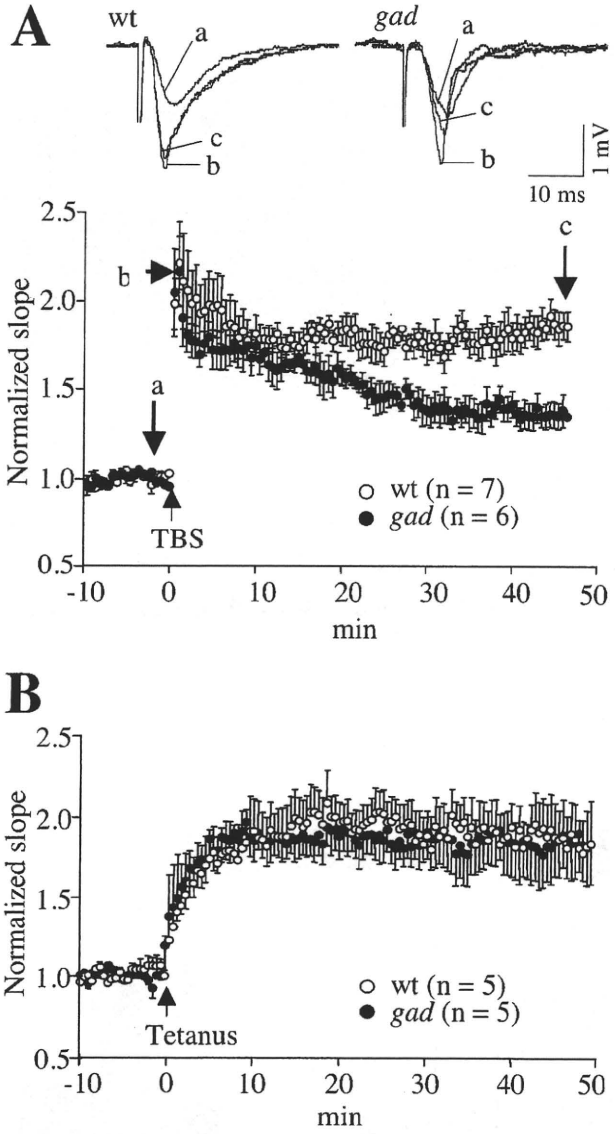

FIG. 4. TBS-induced LTP in area CA1 of the *gad* mouse hippocampus was impaired. (A) LTP induced by TBS in wild-type (○) and *gad* (●) mice. The fEPSP slope was normalized to baseline (pre-TBS) values. Typical fEPSP traces are shown above. Traces were recorded (a) just before TBS, (b) immediately after TBS and (c) 45 min after TBS. (B) Tetanus-induced LTP was identical in wild-type and *gad* mice.

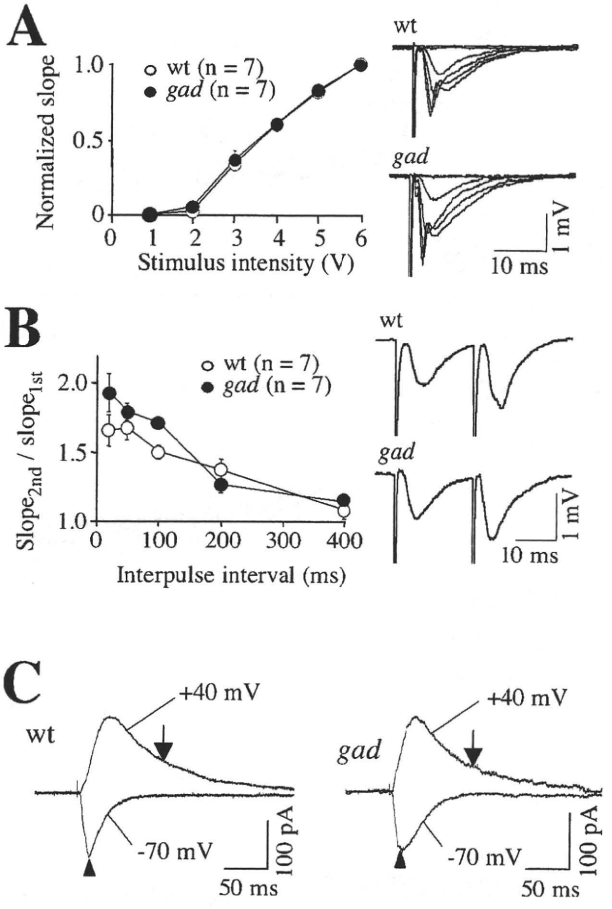

FIG. 5. Stimulus–output curves, paired-pulse facilitation and NMDA receptor-mediated currents were similar in wild-type and *gad* mice. (A) The relation between stimulus intensity and the slope of the fEPSP was identical in wild-type and *gad* mice. For each slice, fEPSP slopes elicited by six different stimulus intensities (1–6 V; sample traces in the right panel) were normalized to the value obtained using 6-V stimulation, and then normalized values were averaged. (B) Paired-pulse facilitation of fEPSPs did not differ substantially between wild-type and *gad* mice. (C) The ratio of NMDA receptor-mediated currents to non-NMDA receptor-mediated currents was identical in wild-type and *gad* mice. Patch-clamp recordings from neurons voltage-clamped to −70 and +40 mV. The arrowhead indicates the peak of the non-NMDA receptor-mediated current, and the arrow indicates 100 ms poststimulation for the NMDA receptor-mediated current; current amplitudes at these points were used for the ratio.

post-TBS was 1.43 ± 0.07 (n = 5) in the presence of actinomycin D, and this value differed significantly from that in wild-type hippocampal slices without actinomycin D (1.87 ± 0.08, P = 0.003; two-tailed Student's t-test). This result agrees with a previous report (Nguyen & Kandel, 1997). In contrast, TBS-induced LTP in *gad* mice was insensitive to actinomycin D (Fig. 6B). The normalized fEPSP slope at 45 min post-TBS was 1.36 ± 0.04 (n = 5) in the presence of actinomycin D and did not differ significantly from the value in *gad* hippocampal slices without actinomycin D (1.36 ± 0.07, P = 0.948; two-tailed Student's t-test). These results suggest that a transcription-dependent component of LTP is impaired in *gad* mice. In both wild-type and *gad* mice, actinomycin D did not affect the baseline fEPSP slope (without TBS) up to 80 min postapplication (Fig. 6C and D).

CREB phosphorylation was altered in gad mice

Late-phase LTP in the hippocampal CA1 field requires transcription elicited by phosphorylation of serine 133 on cAMP response element binding protein (CREB; Nguyen *et al.*, 1994). In addition, Aplysia UCH is involved in persistent activation of PKA during long-term synaptic facilitation (Hedge *et al.*, 1997). From these reports and our experiments using actinomycin D above, we suspected that phosphorylated CREB (pCREB)-induced transcription is disrupted in *gad* mice. To address this, we analysed pCREB in the CA1 field of slices used

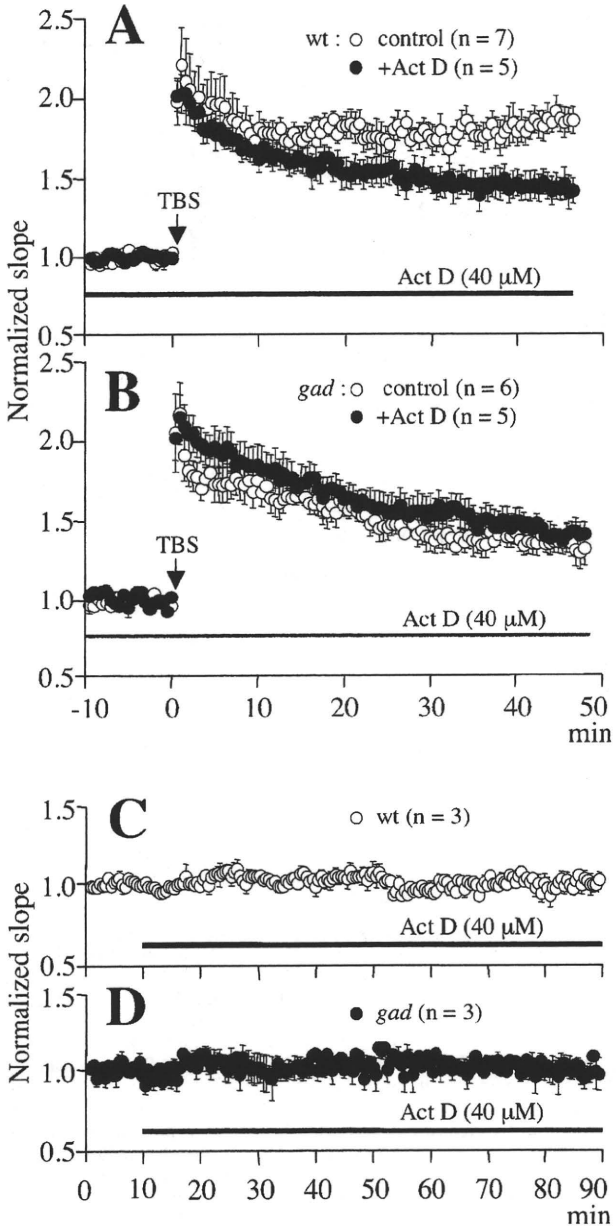

FIG. 6. Transcription-dependent LTP was impaired in *gad* mice. (A and B) Actinomycin D (Act D) suppressed late-phase LTP in (A) wild-type mice but (B) had no effect in *gad* mice. Act D was applied 10 min before LTP induction and was continuously applied until 50 min post-TBS. LTP in the absence of Act D (control) has been reproduced from Fig. 4. (C and D) Without TBS, Act D had no effect on the normalized fEPSP slope in either (C) wild-type or (D) *gad* mice.

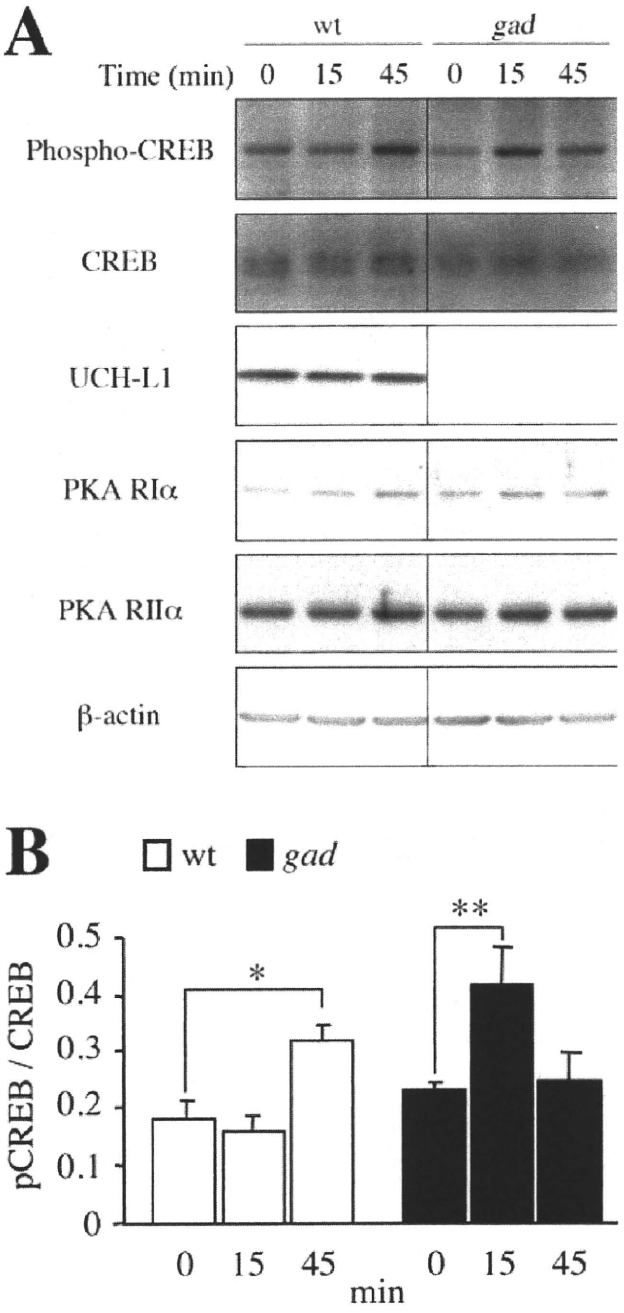

FIG. 7. CREB phosphorylation was altered in *gad* mice. (A) Western blotting of samples prepared from hippocampal slices recovered pre-TBS (0), 15 min post-TBS (15) or 45 min post-TBS (45). Primary antibodies are indicated to the left of the blots. Similar results were obtained at each time point in six slices from wild-type mice and five slices from *gad* mice. (B) The normalized band density of pCREB to CREB at time 0 (pre-TBS), 15 min and 45 min post-TBS in wild-type ($n = 5$) and *gad* ($n = 4$) mice. *$P = 0.012$ and **$P = 0.014$, Bonferroni–Dunn test.

for electrophysiological recording by Western blotting (Fig. 7A). In wild-type mice, pCREB levels at 15 min post-TBS did not differ from pre-TBS levels, but at 45 min post-TBS levels were increased relative to pre-TBS levels. The onset of CREB phosphorylation (45 min postconditioning) is in agreement with a previous report (Ahmed & Frey, 2005). In *gad* mice, however, pCREB levels were increased at 15 min post-TBS but not maintained at 45 min post-TBS (Fig. 7A). Unphosphorylated CREB levels were similar among samples (Fig. 7A). Similar results were obtained in slices from five wild-type and four *gad* mice. In each set of slices, the band density of pCREB was normalized to that of CREB and the values were averaged (Fig. 7B). In wild-type mice (Fig. 7B), the normalized pCREB levels at 15 min post-TBS did not differ significantly from pre-TBS levels

($P = 0.656$; Bonferroni–Dunn test) but at 45 min post-TBS pCREB levels were significantly higher than pre-TBS levels ($P = 0.012$). In *gad* mice (Fig. 7B), pCREB levels were significantly higher at 15 min post-TBS ($P = 0.014$), but at 45 min post-TBS pCREB levels were not significantly different from pre-TBS levels ($P = 0.393$). These results suggest that the onset and persistence of CREB phosphorylation are altered in *gad* mice.

In Aplysia, serotonin stimulation that induces synaptic plasticity increases expression of UCH by about five-fold. The increased UCH expression stimulates proteasomal degradation of the PKA regulatory subunit N4, thereby inducing persistent PKA activity (Hedge *et al.*, 1997). To determine whether this process also exists in mice, we analysed UCH-L1 and PKA regulatory subunits Iα and IIα in the CA1 field of hippocampal slices by Western blotting. As Fig. 7A shows, the level of UCH-L1 was not obviously affected by TBS at either 15 or 45 min post-TBS in wild-type mice. For quantitative analysis, the band density of UCH-L1 was normalized to that of β-actin and the normalized value was then further normalized to pre-TBS values. At 15 and 45 min post-TBS, the normalized values were 1.00 ± 0.24 ($n = 5$) and 1.06 ± 0.21 ($n = 5$), respectively, confirming that UCH-L1 levels were unchanged. Similarly, TBS-induced changes in the levels of PKA regulatory subunit Iα and IIα were also not apparent in either type of mouse (Fig. 7A). For example, the relative band-density of PKA IIα normalized to β-actin was 1.03 ± 0.14 (15 min post-TBS) and 1.06 ± 0.12 (45 min post-TBS) for wild-type mice ($n = 5$). In *gad* mice ($n = 4$), values were 1.02 ± 0.20 (15 min post-TBS) and 1.01 ± 0.25 (45 min post-TBS). For pre-TBS, the relative band-density of PKA IIα normalized to β-actin also did not differ between wild-type and *gad* mice [the normalized value for *gad* mice/the normalized value for wild-type mice was 0.96 ± 0.10 ($n = 4$)].

Discussion

In this study, we demonstrated that UCH-L1 is required for (i) maintenance of memory in a passive avoidance test and exploratory behaviour in a novel environment, and (ii) a transcription-dependent component of TBS-induced LTP in area CA1 of the hippocampus. UCH-L1 may be essential in transcription-dependent TBS-LTP because it maintains the integrity of TBS-induced CREB phosphorylation. No outstanding forebrain atrophy or aberrant structures were evident in 6-week-old *gad* mice at the level of the light microscope. Thus, the functional abnormalities caused by the lack of UCH-L1 occurred in the absence of any detectable gross structural abnormalities in the brain. However, abnormalities in neuron morphology, such as spine morphology or density, remain a possibility in *gad* mice.

Several studies suggest that synaptic and memory abnormalities precede neuronal cell death in AD (Yao *et al.*, 2003) and in AD model mice (Chapman *et al.*, 1999; Freir *et al.*, 2001; Snyder *et al.*, 2005; Shemer *et al.*, 2006), which supports the hypothesis that synapses may be an initial target in AD (Small *et al.*, 2001; Selkoe, 2002). Aβ is thought to be one of the major players that disrupt synaptic function (reviewed in Selkoe, 2002). Because we have shown here that UCH-L1 is essential for memory maintenance, exploratory behaviour and a particular form of hippocampal LTP, it is possible that the AD-associated reduction in UCH-L1 (Choi *et al.*, 2004) further exacerbates the synaptic and memory deficits induced by Aβ accumulation. In addition, glutamate-induced CREB phosphorylation is decreased by Aβ treatment of cultured hippocampal neurons (Vitolo *et al.*, 2002). Thus, accumulation of Aβ and reduction of UCH-L1 may act cooperatively to disrupt CREB phosphorylation. The recent finding that introduction of exogenous UCH-L1 into AD model mice rescues synaptic and memory deficits supports this possibility (Gong *et al.*, 2006).

It should be noted that memory deficits are already evident in young *gad* mice (6 weeks of age). Analysis of AD model mice has shown that the onset of the behavioural phenotype is generally much slower. For example, deficits in visible platform recognition become evident by 9 months of age, and deficits in sensorimotor tasks are clearly manifest by 14 months in the Tg2579 transgenic AD model mice (King & Arendash, 2002). Impairments in passive avoidance and small-pool performance are marked only at 18 and 25 months of age in the APP23 transgenic AD model mice (Kelly *et al.*, 2003). It has not been reported whether UCH-L1 is down-regulated in these model mice. In the APP/PS1 mouse model of AD, on the other hand, relatively young (3- to 4-month-old) mice have impaired contextual learning (Trinchese *et al.*, 2004; Gong *et al.*, 2006), and reduced hippocampal UCH activity is evident at 4–6 months of age (Gong *et al.*, 2006). Whether the onset of the reduction in the hydrolase activity is synchronous with the onset of impaired contextual learning in the APP/PS1 mouse is unknown. This information is necessary to further verify the involvement of UCH-L1 in memory deficits associated with AD and in AD model mice.

Impairment of memory in *gad* mice was associated with impaired transcription-dependent LTP in the hippocampus. Because LTP is a well-known cellular mechanism of memory (reviewed in Bliss & Collingridge, 1993), it is reasonable to speculate that impaired LTP is one of the mechanisms underlying the memory deficits in *gad* mice. Our results provide a possible mechanistic link between the lack of UCH-L1 and impaired LTP: alteration of CREB phosphorylation. Proper timing and persistence of CREB phosphorylation are essential for the gene expression required to maintain LTP in area CA1 of the hippocampus (Impey *et al.*, 1996). After conditioning in the passive avoidance test, cAMP response element-mediated transcription is induced in hippocampal area CA1 (Impey *et al.*, 1998). Thus, the alteration of CREB phosphorylation and subsequent failure to maintain LTP might be responsible for reduced performance of *gad* mice in the passive avoidance test. However, LTP at hippocampal CA1 synapses is dependent on NMDA receptors (Harris *et al.*, 1984; Larson & Lynch, 1988). Phosphorylation of CREB is also NMDA receptor-dependent (Ahmed & Frey, 2005). This type of LTP occurs in various brain regions (reviewed in Martin *et al.*, 2000), and UCH-L1 is expressed in almost all brain regions. Therefore, impaired LTP in other brain regions may also be involved in the poor performance of *gad* mice in the passive avoidance test and other behavioural tests. Postsynaptically, the ubiquitin–proteasome system is involved in activity-dependent changes in postsynaptic protein composition and signalling (Ehlers, 2003; reviewed in Yi & Ehlers, 2007). UCH-L1 has *in vitro* enzymatic activity that exposes the free C-terminus of ubiquitin, which is required for protein ubiquitination (Larsen *et al.*, 1998), and monoubiquitin levels are decreased in *gad* mouse brain (Osaka *et al.*, 2003).

In conclusion, we report that UCH-L1 is required for the maintenance of memory in passive avoidance learning, exploratory behaviour and hippocampal CA1 LTP in mice. We propose that UCH-L1-mediated maintenance of the temporal integrity and persistence of CREB phosphorylation is required for CA1 LTP.

Acknowledgements

We thank Drs Chiaki Itami and Shun Nakamura for their advice in the early stage of this work. We also thank Miss Hisae Kikuchi for her technical assistance. This work was supported in part by Grants-in-Aid for Scientific

Research from the Ministry of Health, Labour and Welfare of Japan, Grants-in-Aid for Scientific Research from the Ministry of Education, Culture, Sports, Science and Technology of Japan, the Program for Promotion of Fundamental Studies in Health Sciences of the National Institute of Biomedical Innovation, and a grant from the Japan Science and Technology Agency.

Abbreviations

Aβ, amyloid β-protein; ACSF, artificial cerebrospinal fluid; AD, Alzheimer's disease; CREB, cyclic AMP response element-binding protein; fEPSPs, field excitatory postsynaptic potentials; *gad*, gracile axonal dystrophy; H&E, hematoxylin and eosin; LTP, long-term potentiation; pCREB, phosphorylated CREB; PD, Parkinson's disease; PKA, protein kinase A; TBS, theta-burst stimulation; UCH-L1, ubiquitin C-terminal hydrolase L1.

References

Abel, T., Nguyen, P.V., Barad, M., Deuel, T.A. & Kandel, E.R. (1997) Genetic demonstration of a role for PKA in the late phase of LTP and in the hippocampus-based long-term memory. *Cell*, **88**, 615–626.

Ahmed, T. & Frey, J.U. (2005) Plasticity-specific phosphorylation of CaMKII, MAP-kinases and CREB during late-LTP in rat hippocampal slices in vitro. *Neuropharmacology*, **49**, 477–492.

Bevilaqua, L., Ardenghi, P., Schroder, N., Bromberg, E., Schmitz, P.K., Schaeffer, E., Quevedo, J., Bianchin, M., Walz, R., Medina, J.H. & Izquierdo, I. (1997) Drugs acting upon the cyclic adenosine monophosphate/protein kinase A signaling pathway modulate memory consolidation when given late after training into rat hippocampus but not amygdala. *Behav. Pharmacol.*, **8**, 331–338.

Bliss, T.V. & Collingridge, G.L. (1993) A synaptic model of memory: long-term potentiation in the hippocampus. *Nature*, **361**, 31–39.

Bouton, M.E., Kenney, F.A. & Rosengard, C. (1990) State-dependent fear extinction with two benzodiazepine tranquilizers. *Behav. Neurosci.*, **104**, 44–55.

Bradshaw, K.D., Emptage, N.L. & Bliss, T.V. (2003) A role for dendritic protein synthesis in hippocampal late LTP. *Eur. J. Neurosci.*, **18**, 3150–3152.

Castegna, A., Aksenov, M., Aksenova, M., Thongboonkerd, V., Klein, J.B., Pierce, W.M., Booze, R., Markesbery, W.M. & Butterfield, D.A. (2002) Proteomic identification of oxidatively modified proteins in Alzheimer's disease brain. Part I: creatine kinase BB, glutamine synthase, and ubiquitin carboxy-terminal hydrolase L-1. *Free Radic. Biol. Med.*, **33**, 562–571.

Chapman, P.F., White, G.L., Jones, M.W., Cooper-Blacketer, D., Marshall, V.J., Irizarry, M., Younkin, L., Good, M.A., Bliss, T.V., Hyman, B.T., Younkin, S.G. & Hsiao, K.K. (1999) Impaired synaptic plasticity and learning in aged amyloid precursor protein transgenic mice. *Nat. Neurosci.*, **2**, 271–276.

Choi, J., Levey, A.I., Weintraub, S.T., Rees, H.D., Gearing, M., Chin, L.S. & Li, L. (2004) Oxidative modifications and down-regulation of ubiquitin carbocyl-terminal hydrolase L1 associated with idiopathic Parkinson's and Alzheimer's diseases. *J. Biol. Chem.*, **279**, 13256–13264.

Ehlers, M.D. (2003) Activity level controls postsynaptic composition and signaling via the ubiquitin-proteasome system. *Nat. Neurosci.*, **6**, 231–242.

Freir, D.B., Holscher, C. & Herron, C.E. (2001) Blockade of long-term potentiation by β-amyloid peptides in the CA1 region of the rat hippocampus in vivo. *J. Neurophysiol.*, **85**, 708–713.

Gong, B., Cao, Z., Zheng, P., Vitolo, O.V., Liu, S., Staniszewski, A., Moolman, D., Zhang, H., Shelanski, M. & Arancio, O. (2006) Ubiquitin hydrolase Uch-L1 rescues beta-amyloid-induced decreases in synaptic function and contextual memory. *Cell*, **126**, 775–788.

Harris, E.W., Ganong, A.H. & Cotman, C.W. (1984) Long-term potentiation in the hippocampus involves activation of N-methyl-D-aspartate receptors. *Brain Res.*, **323**, 132–137.

Hedge, A.N., Inokuchi, K., Pei, W., Casadio, A., Ghirardi, M., Chain, D.G., Martin, K.C., Kandel, E.R. & Schwartz, J.H. (1997) Ubiquitin C-terminal hydrolase is an immediate-early gene essential for long-term facilitation in Aplysia. *Cell*, **89**, 115–126.

Ichihara, N., Wu, J., Chui, D.H., Yamazaki, K., Wakabayashi, T. & Kikuchi, T. (1995) Axonal degeneration promotes abnormal accumulation of amyloid beta-protein in ascending gracile tract of gracile axonal dystrophy (*GAD*) mouse. *Brain Res.*, **695**, 173–178.

Impey, S., Mark, M., Villacres, E.C., Poser, S., Chavkin, C. & Storm, D.R. (1996) Induction of CRE-mediated gene expression by stimuli that generate long-lasting LTP in area CA1 of the hippocampus. *Neuron*, **16**, 973–982.

Impey, S., Smith, D.M., Obrietan, K., Donahue, R., Wade, C. & Storm, D.R. (1998) Stimulation of cAMP response element (CRE)-mediated transcription during contextual learning. *Nat. Neurosci.*, **1**, 595–601.

Kabuta, T., Suzuki, Y. & Wada, K. (2006) Degradation of amyotrophic lateral sclerosis-linked mutant Cu, Zn-superoxide dismutase proteins by macro-autophagy and the proteasome. *J. Biol. Chem.*, **281**, 30524–30533.

Kelly, P.H., Bondolfi, L., Hunziker, D., Schlecht, H.-P., Carver, K., Maguire, E., Arbamowski, D., Wiederhold, K.-H., Sturchler-Pierrat, C., Jucker, M., Bergmann, R., Staufenbiel, M. & Sommer, B. (2003) Progressive age-related impairment of cognitive behavior in APP23 transgenic mice. *Neurobiol. Aging*, **24**, 365–378.

Kikuchi, T., Mukoyama, M., Yamazaki, K. & Moriya, H. (1990) Axonal degeneration of ascending sensory neurons in gracile axonal dystrophy mutant mouse. *Acta Neuropathol.*, **80**, 145–151.

King, D.L. & Arendash, G.W. (2002) Behavioral characterization of the Tg2576 transgenic model of Alzheimer's disease through 19 months. *Physiol. Behav.*, **75**, 627–642.

Larsen, C.N., Krantz, B.A. & Wilkinson, K.D. (1998) Substrate specificity of deubiquitinating enzyme: ubiquitin C-terminal hydrolases. *Biochemistry*, **37**, 3358–3368.

Larson, J. & Lynch, G. (1988) Role of N-methyl-D-aspartate receptors in the induction of synaptic potentiation by burst stimulation patterned after the hippocampal theta-rhythm. *Brain Res.*, **441**, 111–118.

Leroy, E., Boyer, R., Auburger, G., Leube, B., Ulm, G., Mezey, E., Harta, G., Brownstein, M.J., Jonnalagada, S., Chernova, T., Dehejia, A., Lavedan, C., Gasser, T., Steinbach, P.J., Wilkinson, K.D. & Polymeropoulos, M.H. (1998) The ubiquitin pathway in Parkinson's disease. *Nature*, **395**, 451–452.

Lever, C., Burton, S. & O'Keefe, L. (2006) Rearing on hind legs, environmental novelty, and the hippocampal formation. *Rev. Neurosci.*, **17**, 111–133.

Liu, Y.C., Fallon, L., Lashuei, H.A., Liu, Z.H. & Lansbury,P.T. Jr (2002) The UCH-L1 gene encodes two opposing enzymatic activities that affect alpha-synuclein degradation and Parkinson's disease susceptibility. *Cell*, **111**, 209–218.

Malinow, R. & Malenka, R.C. (2002) AMPA receptor trafficking and synaptic plasticity. *Annu. Rev. Neurosci.*, **25**, 103–126.

Maraganore, D.M., Farrer, M.J., Hardly, J.A., Lincoln, S.J., McDonnell, S.K. & Rocca, W.A. (1999) Case-control study of the ubiquitin carboxy-terminal hydrolase L1 gene in Parkinson's disease. *Neurology*, **53**, 1858–1860.

Martin, S.J., Grimwood, P.D. & Morris, R.G.M. (2000) Synaptic plasticity and memory. *Annu. Rev. Neurosci.*, **23**, 649–711.

Morris, R.G., Garrud, P., Rawlins, J.N. & O'Keefe, J. (1982) Place navigation impaired in rats with hippocampal lesions. *Nature*, **297**, 681–683.

Nguyen, P.V., Abel, T. & Kandel, E.R. (1994) Requirement of a critical period of transcription for induction of a late phase of LTP. *Science*, **265**, 1104–1107.

Nguyen, P.V., Duffy, S.N. & Young, J.Z. (2000) Differential maintenance and frequency-dependent tuning of LTP at hippocampal synapses of specific strains of inbred mice. *J. Neurophysiol.*, **84**, 2484–2493.

Nguyen, P.V. & Kandel, E.R. (1997) Brief theta-burst stimulation induces a transcription-dependent late phase of LTP requiring cAMP in area CA1 of the mouse hippocampus. *Learn. Mem.*, **4**, 230–243.

Osaka, H., Wang, Y.-L., Takada, K., Takizawa, S., Setsuie, R., Li, H., Sato, Y., Nishikawa, K., Sun, Y.-J., Sakurai, M., Harada, T., Hara, Y., Kimura, I., Chiba, S., Namikawa, K., Kiyama, H., Noda, M., Aoki, S. & Wada, K. (2003) Ubiquitin carboxy-terminal hydrolase L1 binds to and stabilizes monoubiquitin in neuron. *Human Mol. Genet.*, **12**, 1945–1958.

Saigoh, K., Wang, Y.-L., Suh, J.G., Yamanishi, T., Sakai, Y., Kiyosawa, H., Harada, T., Ichihara, N., Wakana, S., Kikuchi, T. & Wada, K. (1999) Intragenic deletion in the gene encoding ubiquitin carboxy-terminal hydrolase in *gad* mice. *Nat. Genet.*, **23**, 47–51.

Selkoe, D.J. (2002) Alzheimer's disease is a synaptic failure. *Science*, **298**, 789–791.

Shemer, I., Holmgren, C., Min, R., Fulop, L., Zilberter, M., Sousa, K.M., Farkas, T., Hartig, W., Penke, B., Burnashev, N., Tanila, H., Zilberter, Y. & Harkany, T. (2006) Non-fibrillar β-amyloid abates spike-timing-dependent synaptic potentiation at excitatory synapses in layer 2/3 of the neocortex by targeting postsynaptic AMPA receptors. *Eur. J. Neurosci.*, **23**, 2035–2047.

Small, D.H., Mok, S.S. & Bornstein, J.C. (2001) Alzheimer's disease and Aβ toxicity: from top to bottom. *Nat. Rev. Neurosci.*, **2**, 595–598.

Snyder, E.M., Nong, Y., Almeida, C.G., Paul, S., Moran, T., Choi, E.Y., Nairn, A.C., Salter, A.W., Lombroso, P.J., Gouras, G.K. & Greengard, P. (2005) Regulation of NMDA receptor trafficking by amyloid-β. *Nat. Neurosci.*, **8**, 1051–1058.

Takamatsu, I., Sekiguchi, M., Wada, K., Sato, T. & Ozaki, M. (2005) Propofol-mediated impairment of CA1 long-term potentiation in mouse hippocampal slices. *Neurosci. Lett.*, **389**, 129–132.

Trinchese, F., Liu, S., Battaglia, F., Walter, S., Mathews, P.M. & Arancio, O. (2004) Progressive age-related development of Alzheimer-like pathology in APP//PS1 mice. *Ann. Neurol.*, **55**, 801–814.

Vitolo, O.V., Sant'Angelo, A., Costanzo, V., Battaglia, F., Arancio, O. & Shelanski, M. (2002) Amyloid β-peptide inhibition of the PKA/CREB pathway and long-term potentiation: reversibility by drugs that enhance cAMP signaling. *Proc. Natl. Acad. Sci. USA*, **99**, 13217–13221.

Wilkinson, K.D., Lee, K.M., Deshpande, S., Duerksen-Hughes, P., Boss, J.M. & Pohl, J. (1989) The neuron-specific protein PGP 9.5 is a ubiquitin carboxyl-terminal hydrolase. *Science*, **246**, 670–673.

Xue, S. & Jia, J. (2006) Genetic association between ubiquitin carboxy-terminal hydrolase-L1 gene S18Y polymorphism and sporadic Alzheimer's disease in a Chinese Han population. *Brain Res.*, **1087**, 28–32.

Yamada, K., Santo-Yamada, Y. & Wada, K. (2003) Stress-induced impairment of inhibitory avoidance learning in female neuromedin B receptor-deficient mice. *Physiol. Behav.*, **78**, 303–309.

Yamada, K., Santo-Yamada, Y., Wada, E. & Wada, K. (2002) Role of bombesin (BN)-like peptides/receptors in emotional behavior by comparison of three strains of BN-like peptide receptor knockout mice. *Mol. Psychiatry*, **7**, 113–117.

Yao, P.J., Zhu, M., Pyun, E.I., Brooks, A.I., Therianos, S., Meyers, V.E. & Coleman, P.D. (2003) Defects in expression of genes related to synaptic vesicle trafficking in frontal cortex of Alzheimer's disease. *Neurobiol. Dis.*, **12**, 97–109.

Yi, J.J. & Ehlers, M.D. (2007) Emerging roles for ubiquitin and protein degradation in neuronal function. *Pharmacol. Rev.*, **59**, 14–39.

Zushida, K., Sakurai, M., Wada, K. & Sekiguchi, M. (2007) Facilitation of extinction learning for contextual fear memory by PEPA-a potentiator of AMPA receptors. *J. Neurosci.*, **27**, 158–166.

Available online at www.sciencedirect.com
ScienceDirect
Neuroscience Research 61 (2008) 143–158
Neuroscience Research
www.elsevier.com/locate/neures

Behavioral and gene expression analyses of *Wfs1* knockout mice as a possible animal model of mood disorder

Tadafumi Kato [a,*], Mizuho Ishiwata [a], Kazuyuki Yamada [b], Takaoki Kasahara [a], Chihiro Kakiuchi [a], Kazuya Iwamoto [a], Koki Kawamura [c], Hisamitsu Ishihara [d], Yoshitomo Oka [d]

[a] *Laboratory for Molecular Dynamics of Mental Disorders, RIKEN Brain Science Institute, Hirosawa 2-1, Wako, Saitama 351-0198, Japan*
[b] *Support Unit for Animal Experiment, RIKEN Brain Science Institute, Wako, Saitama 351-0198, Japan*
[c] *Laboratory for Cell Culture Development, RIKEN Brain Science Institute, Wako, Saitama 351-0198, Japan*
[d] *Division of Molecular Metabolism and Diabetes, Tohoku University Graduate School of Medicine, Sendai, Japan*

Received 21 November 2007; accepted 7 February 2008
Available online 14 February 2008

Abstract

Wolfram disease is a rare genetic disorder frequently accompanying depression and psychosis. Non-symptomatic mutation carriers also have higher rates of depression and suicide. Because *WfS1*, the causative gene of Wolfram disease, is located at 4p16, a linkage locus for bipolar disorder, mutations of *WfS1* were suggested to be involved in the pathophysiology of bipolar disorder. In this study, we performed behavioral and gene expression analyses of *Wfs1* knockout mice to assess the validity as an animal model of mood disorder. In addition, the distribution of *Wfs1* protein was examined in mouse brain. *Wfs1* knockout mice did not show abnormalities in circadian rhythm and periodic fluctuation of wheel-running activity. Behavioral analysis showed that *Wfs1* knockout mice had retardation in emotionally triggered behavior, decreased social interaction, and altered behavioral despair depending on experimental conditions. *Wfs1*-like immunoreactivity in mouse brain showed a similar distribution pattern to that in rats, including several nuclei potentially relevant to the symptoms of mood disorders. Gene expression analysis showed down-regulation of *Cdc42ep5* and *Rnd1*, both of which are related to Rho GTPase, which plays a role in dendrite development. These findings may be relevant to the mood disorder observed in patients with Wolfram disease.

Keywords: Wolframin; Wolfram disease; Depression; Bipolar disorder; DNA microarray; Forced swimming test

1. Introduction

Wolfram disease (Online Mendelian Inheritance in Man [OMIM] 222300) is a rare autosomal recessive neurodegenerative disorder characterized by early-onset diabetes mellitus, progressive optic atrophy, diabetes insipidus, and deafness (Domenech et al., 2006); *WfS1/wolframin* has been identified as the causative gene (Strom et al., 1998; Inoue et al., 1998). Approximately, 60% of the patients with Wolfram disease have mental symptoms, such as severe depression, psychosis, impulsivity, and aggression (Swift et al., 1990). More importantly, carriers of *WfS1* mutations, who are not affected with Wolfram disease, have a 26-fold higher likelihood of psychiatric hospitalization mainly due to depression (Swift and Swift, 2000). The *WfS1* gene locates at 4p16.1 (Strom et al., 1998; Inoue et al., 1998), a replicated linkage locus of bipolar disorder (Ewald et al., 1998, 2002; Detera-Wadleigh et al., 1999). Some studies showed that bipolar disorder with psychosis (Als et al., 2004; Cheng et al., 2006) or suicidal behavior (Cheng et al., 2006) is linked with this locus. These lines of evidence suggested the possible role of *WfS1* mutations in the pathophysiology of bipolar disorder and related phenotypes.

To date, mutation screening of the *WfS1* gene has been reported in 84 patients with bipolar disorder, 54 with major depression, 119 with schizophrenia, 100 suicide victims, 3 with schizoaffective disorder, and several other patients with other psychiatric diagnoses (Ohtsuki et al., 2000; Martorell et al., 2003; Torres et al., 2001; Crawford et al., 2002; Evans et al., 2000). However, none of these patients had mutations causing Worfram disease.

* Corresponding author. Tel.: +81 48 467 6949; fax: +81 48 467 6947.
E-mail address: kato@brain.riken.jp (T. Kato).

0168-0102/$ – see front matter © 2008 Published by Elsevier Ireland Ltd and the Japan Neuroscience Society.
doi:10.1016/j.neures.2008.02.002

Despite the fact that *WfS1* mutations may not be a frequent cause of mental disorders, the mechanism underlying how *WfS1* mutations lead to mental symptoms in patients with Wolfram disease will shed light on the pathophysiology of mood disorders. Mice lacking the *Wfs1* gene might be useful as a genetic animal model of mood disorders.

The symptoms of Wolfram disease resemble those of mitochondrial diseases and, indeed, initial studies suggested mitochondrial dysfunction in Wolfram disease based on mitochondrial DNA (mtDNA) deletions found in patients (Rotig et al., 1993). However, the protein coded by *WfS1* was found to be localized in endoplasmic reticulum (ER) (Takeda et al., 2001; Philbrook et al., 2005). *WfS1* expression was induced by ER stress (Fonseca et al., 2005) or *XBP1* overexpression (Kakiuchi et al., 2006), and disruption of *Wfs1* caused a dysfunctional ER stress response (Fonseca et al., 2005; Riggs et al., 2005; Yamada et al., 2006). Recent studies have provided insight into the function of *WfS1* protein; *WfS1* induces cation channel activity on ER membranes (Osman et al., 2003) and regulates calcium levels in ER (Takei et al., 2006). It also plays a role in stimulus-secretion coupling for insulin exocytosis in pancreatic β cells (Ishihara et al., 2004). Disruption of *Wfs1* increased vulnerability to cell death in the knockout (KO) mice (Ishihara et al., 2004; Philbrook et al., 2005; Riggs et al., 2005; Yamada et al., 2006). In the rat brain, *WfS1* was distributed predominantly in neurons of the so-called limbic system (Takeda et al., 2001). *WfS1* mutations could lead to loss of *WfS1*-expressing neurons in particular brain regions of patients with Wolfram disease, which may underlie progression of mental symptoms.

In this study, we performed behavioral analysis of *Wfs1* KO mice to characterize their behavioral abnormality. We previously developed neuron-specific mutant polymerase γ-transgenic mice (mPolg Tg mice) based on a mitochondrial dysfunction hypothesis of bipolar disorder (Kato and Kato, 2000) and demonstrated that these mice had bipolar disorder-like phenotypes, such as altered circadian rhythm and periodic fluctuation of wheel-running activity (Kasahara et al., 2006). Whether or not the *Wfs1* KO mice show such wheel-running activity was examined. A behavioral test battery was also conducted to search for other behavioral phenotypes. Distribution of *Wfs1* in the brain was examined to search for the neural basis of behavioral alteration. In addition, gene expression analysis was performed to search for the molecular basis of behavioral phenotypes of *Wfs1* KO mice.

2. Experimental procedures

2.1. Generation of Wfs1 KO mice

The methods for the generation of *Wfs1* KO mice have been described elsewhere (Ishihara et al., 2004). In brief, a neomycin-resistance gene was inserted into exon 2 of the *Wfs1* gene in the targeting vector. The targeting vector was injected into 129Sv embryonic stem (ES) cells, and the ES cells with homologous recombination were obtained. By crossing the chimeric mice with C57BL/6J (B6) mice, *Wfs1* heterozygous KO mice were obtained. Genotyping was performed as previously described (Ishihara et al., 2004). The heterozygous KO mice were crossed with the B6 mice for at least eight generations before the analysis. The mice were maintained in a 12-h light:12-h dark cycle, except for several specific experiments as indicated. Wild-type (WT) littermates were used for the control whenever possible. All animal experiments were approved by the local animal experiment committees of RIKEN and Behavioral and Medical Sciences Research Consortium (BMSRC) (Akashi, Japan). Animal experiments were carried out in accordance with the National Institute of Health Guide for the Care and Use of Laboratory Animals. All efforts were made to minimize the number of animals used and their suffering.

2.2. Wheel-running activity

For this analysis, 11 homozygous KO mice ($Wfs1^{-/-}$) and 9 WT littermates ($Wfs1^{+/+}$) were used. All were males aged 34 weeks at the initiation of the analysis. The groups did not differ significantly in body weight.

The methods for the analysis of wheel-running activity were described in detail elsewhere (Kasahara et al., 2006). In brief, mice were individually housed in cages (width, 24 cm; depth, 11 cm; height, 14 cm) equipped with a steel wheel (width, 5 cm; diameter, 14 cm) (O'Hara & Co., Tokyo, Japan). Wheel-running activity was monitored by measuring the rotation of the wheel (3 counts/1 rotation). Food and water were available ad libitum. The data of initial 7–10 days were omitted from the analysis. Delayed and anticipatory activity indices, referring to the wheel-running activity during the initial 3 h of a light phase and that during the last 3 h of a light phase, were calculated. The periodicity of wheel-running activity was assessed by Lomb-Scargle periodogram (Kasahara et al., 2006).

The Mann–Whitney *U*-test was used for statistical analyses. Significance levels were set at 0.05 (two-tailed; d.f., degree of freedom). The average and standard error of mean (S.E.M.) were presented for each experimental parameter in one group.

2.3. Behavioral analysis: phase I. Screening by a test battery

This analysis was performed at BMSRC (Akashi, Japan). For this analysis, 14 homozygous KO mice ($Wfs1^{-/-}$), 14 heterozygous KO mice ($Wfs1^{-/+}$), and 13 WT littermates ($Wfs1^{+/+}$) were analyzed. All were males aged 12 weeks at the initiation of the behavioral analysis. The analyses were performed in the order of open-field test, startle response and prepulse inhibition test, elevated plus maze, Morris water maze, passive avoidance learning, active avoidance learning, and forced swimming test. After the behavioral test battery, the non-fasting blood glucose level was examined to rule out the possibility that elevated blood glucose levels might affect the results of behavioral analysis. There was no significant difference among the genotypes, consistent with a previous report that there was no apparent increase in blood glucose levels in *Wfs1* KO mice on the B6 background (Ishihara et al., 2004).

2.3.1. Open-field test

A transparent cubic box without a ceiling (30 cm × 30 cm × 30 cm) was placed in a ventilated sound-attenuating chamber. A 40-W white lamp provided room lighting, which was approximately 110 lx on the floor of the chamber. In addition, a fan attached on the upper part of the wall at one end of the chamber presented a masking noise of 45 dB. Two infrared beams were set on each wall 2 cm above the floor with an interval of 10 cm. The total number of successive interceptions of two adjoining beams on each bank was scored as locomotion behavior. The other 12 infrared ray beams were attached 4.5 cm above the floor in 2.5-cm intervals, and the total number of vertical beam interceptions was scored as rearing behavior. Each mouse was allowed to explore freely in the open-field area for 20 min.

For statistical analysis, repeated measures analysis of variance (ANOVA) with the intrasubject factor of time (1–20 min) and the intersubject factor of genotype (−/−, +/−, and +/+) was applied.

2.3.2. Startle response and prepulse inhibition (PPI)

Each mouse was enclosed in a transparent acrylic box (7 cm × 7 cm × 10 cm). Startle response was detected as vibration of the box, using an accelerometer (GH-313A, Keyence, Osaka, Japan). The acoustic startle pulse of broadband burst (115 dB, 50 ms) and tone prepulse (85 dB, 30 ms) were presented via a speaker located in front of the box. Light prepulse (30 ms) was

applied by LED. At the beginning of the session, 40 startle pulses were presented to test for basal startle responsiveness and its habituation. The average values of eight blocks, consisting of five startle pulses each, were used for the statistical analysis. After that, three different types of trials were performed: startle pulse alone ($n = 12$), startle pulse preceded by a tone prepulse ($n = 12$), and startle pulse preceded by a light prepulse ($n = 12$). Prepulses were presented 50, 100, or 200 ms before the startle pulse. In total, six types of prepulse ($n = 4$, each) were applied. The mean interval averaged 25 s (15–45 s) throughout the session. The startle response was recorded for 200 ms with the sampling frequency of 1000 Hz. The PPI was assessed by the ratio of the mean response of trials with one type of prepulse ($n = 4$) divided by the mean response of trials without prepulse ($n = 12$). Because light prepulse did not attenuate the startle response at all, only the data of tone prepulse were presented.

2.3.3. Elevated plus maze

The maze consisted of four arms, two open arms and two closed arms, 5 cm wide and 30 cm long with a gray acrylic floor, that met at a 10 cm × 10 cm center zone. Two closed arms had the transparent walls of 15 cm height on both sides, and the open arms had the low walls of 3 mm height on the both sides. The apparatus was mounted 75 cm above the floor of the room. The room lighting was approximately 20 lx on the maze. The video camera was placed 80 cm above the maze. A fan generated a masking noise of 45 dB. The animal was placed gently onto the center of the maze and was allowed to explore the maze freely for 10 min. Number of entries into each arm and time spent in each arm were recorded from videotapes.

2.3.4. Morris water maze

A round pool, with the diameter of 95 cm and the depth of 21.5 cm, was placed in the center of a 140 cm × 130 cm room. A platform with the diameter of 11 cm was set in one of quadrants and 5 mm beneath the surface of black water maintained at 21 ± 1 °C. On the first to fifth days, five trials per day were performed for learning phase. The mouse was released on one of three quadrants of the pool without the platform, and the time to reach the platform was measured. When the mouse could not reach the platform within 60 s, the experimenter placed the mouse on the platform. On the sixth day, a probe test was performed to examine whether the mouse remembered the place of the platform. The mouse was released in the quadrant on the opposite side of the platform and its behavior for 60 s was videotaped. The time staying in the target quadrant, where the platform had been placed, and immobility time were measured.

2.3.5. Passive avoidance learning

A mouse was placed in a box, consisting of two rooms separated by a shutter, that is, light and dark compartments (10 cm × 10 cm each). In the acquisition trial, the mouse was kept in the light compartment. Five seconds later, the door to the dark compartment was opened. When the mouse moved into the dark compartment, the shutter was closed, and 10 s later, an electrical shock (160 V, 3 s) was delivered through the grid floor. Twenty-four hours later, each mouse was placed again in the light compartment and the latency to enter the dark compartment was recorded up to a maximum of 180 s.

2.3.6. Active avoidance learning

The same apparatus with the one used for passive avoidance learning was used, but there was no shutter between the light and dark compartments. The box was set in a soundproof chamber, and illuminated by a 20 W white light set on the chamber. The ceiling of the dark room is made of a black acryl board, and the ceiling of the light room was a transparent acryl board.

The training was performed for 3 days. On each day, one session consisting of 50 trials was performed. In each trial, a condition stimulus (CS) of 1500 Hz sound (85 dB) was followed by an unconditioned stimulus (US) of 140-V electrical shock. The US was given 5 s after the initiation of the CS and continued until the mouse escaped to the other compartment. If the mouse did not move to the other compartment, the US lasted 15 s together with the CS. If the mouse moved within 5 s after the CS, CS was stopped and no US was given. None of the mice experienced the maximum length of the CS. The time from the CS to the escape and the number of escapes were used for the performance of learning.

2.3.7. Forced swimming test

Animals were thrown into a square pool 24 cm × 24 cm in size. The water was maintained constant at 21 °C. On the first day, the mice were left in the pool for 20 min, and the mobility during the first 5 min recorded by videocamera was assessed. On the second day, animals were thrown into the pool for 5 min and the immobility time during the 5 min was recorded. The immobility was defined by the two criteria. (1) No movement of all legs and the tail. (2) Completely stationary state in the pool, or the movement only by inertia by the adjacent movement. The immobility was assessed by three independent raters by scrutinizing the video and the median value of the three raters was used for the analysis.

2.4. Behavioral analysis: phase II

This analysis was performed at the Support Unit for Animal Experiment, RIKEN BSI. For this analysis, 9 homozygous KO mice (*Wfs1*$^{-/-}$) and 11 WT littermates (*Wfs1*$^{+/+}$) were analyzed. All were males aged 31 weeks at the initiation of the behavioral analysis. There was no significant difference of body weight at the initiation of the behavioral tests.

The analyses were performed in the order of home cage activity, open-field test, light-dark (L-D) box test, elevated plus maze, startle response and PPI test, Morris water maze, and fear conditioning. After each trial (except the auditory startle response and the water maze), apparatuses were wiped and cleaned by 80% alcohol and damp towel. For data acquisition, the Image J program (http://rsb.info.Nih.gov/ij) was used after some modification.

2.4.1. Environment of behavioral laboratory and housing condition of mice

Mice were housed individually for several days before they were transferred to the behavioral laboratory. The laboratory was air-conditioned and maintained temperature and humidity within approximately 22–23 °C and 50–55%. Food and water were freely available except during experimentation. Large tweezers were used to handle mice to avoid individual differences in the handling procedure. All of the experiments were conducted in the light phase (9:00–18:00 h), and the starting times of the experiments were kept constant.

2.4.2. Home cage activity measurement

Spontaneous activity of mice in their home cage was measured using a 24-ch ABsystem 4.0 (Neuroscience, Tokyo, Japan). Cages were individually set into the compartments made of stainless steel in the negative pressure rack (JCL, Tokyo, Japan). An infrared sensor was equipped on the ceiling of each compartment and it detected movements of the mice. Home cage activity was measured for 1 week from the afternoon of the day of transferring to the behavioral laboratory (day 1) until the next day of the week (day 8). After the termination of home cage activity measurement, cages and bedding materials were changed to fresh ones and then mice were maintained in the microisolation rack (Allentown Inc., Allentown, PA, USA), the same as those used in breeding rooms throughout the behavioral screening.

2.4.3. Open-field test

Four days after the termination of home cage activity measurement (day 12), an open-field test was conducted. The detailed protocol is shown in the supplementary information.

2.4.4. L-D box test

The next day (day 13) after the open-field test, an L-D box test was conducted. A four-channel of the L-D box system was equipped in the same sound-proof room as the open field. Each light box was made of white plastic (20 cm × 20 cm × 20 cm [H]) and illuminated by LEDs (250 lx at the center of the box); a CCD camera was equipped on the ceiling. Each dark box was made of black plastic (20 cm × 20 cm × 20 cm [H]) and an infrared camera was equipped on the ceiling. There was a tunnel for transition on the center panel between the light box and dark box (3 cm × 5 cm) with an automatic sliding door. In the L-D box test, mice were individually introduced into the light box, and the door of the tunnel automatically opened 3 s after the introduction of a mouse. Then mouse was allowed to move freely in the L-D box for 10 min. Total distance traveled, percent distance traveled in the light